Oncogene (2012) 31, 2017–2027

www.nature.com/onc

ORIGINAL ARTICLE

GATA3 inhibits lysyl oxidase-mediated metastases of human basal triple-negative breast cancer cells

IM Chu[1], AM Michalowski[1], M Hoenerhoff[2], KM Szauter[3], D Luger[1], M Sato[1], K Flanders[1], A Oshima[1], K Csiszar[3] and JE Green[1]

[1]*Laboratory of Cancer Biology and Genetics, National Cancer Institute, Bethesda, MD, USA;* [2]*Cellular and Molecular Pathology Branch, National Toxicology Program, National Institute of Environmental Health Sciences, Research Triangle Park, NC, USA and* [3]*John A Burns School of Medicine, University of Hawaii, Honolulu, HI, USA*

Discovery of mechanisms that impede the aggressive and metastatic phenotype of human basal triple-negative-type breast cancers (BTNBCs) could provide novel targets for therapy for this form of breast cancer that has a relatively poor prognosis. Previous studies have demonstrated that expression of GATA3, the master transcriptional regulator of mammary luminal differentiation, can reduce the tumorigenicity and metastatic propensity of the human BTNBC MDA-MB-231 cell line (MB231), although the mechanism for reduced metastases was not elucidated. We demonstrate through gene expression profiling that GATA3 expression in 231 cells resulted in the dramatic reduction in the expression of lysyl oxidase (LOX), a metastasis-promoting, matrix-remodeling protein, in part, through methylation of the LOX promoter. Suppression of LOX expression by GATA3 was further confirmed in the BTNBC Hs578T cell line. Conversely, reduction of GATA3 expression by small interfering RNA in luminal BT474 cells increased LOX expression. Reconstitution of LOX expression in 231-GATA3 cells restored metastatic propensity. A strong inverse association between LOX and GATA3 expression was confirmed in a panel of 51 human breast cancer cell lines. Similarly, human breast cancer microarray data demonstrated that high LOX/low GATA3 expression is associated with the BTNBC subtype of breast cancer and poor patient prognosis. Expression of GATA3 reprograms BTNBCs to a less aggressive phenotype and inhibits a major mechanism of metastasis through inhibition of LOX. Induction of GATA3 in BTNBC cells or novel approaches that inhibit LOX expression or activity could be important strategies for treating BTNBCs.
Oncogene (2012) **31**, 2017–2027; doi:10.1038/onc.2011.382; published online 5 September 2011

Keywords: GATA3; basal triple-negative breast cancer; lysyl oxidase; differentiation; gene expression profiling

Correspondence: Dr JE Green, Transgenic Oncogenesis and Genomics Section, Laboratory of Cancer Biology and Genetics, National Cancer Institute, Building 37, Room 4054, 37 Convent Dr, Bethesda, MD 20892, USA.
E-mail: jegreen@nih.gov
Received 6 February 2011; revised 19 July 2011; accepted 24 July 2011; published online 5 September 2011

Introduction

Although primary tumors in cancer patients are often successfully treated, the emergence of metastases generally heralds a poor prognosis and is responsible for over 90% of cancer patient deaths (Gupta and Massague, 2006). High-throughput gene expression profiling and molecular subtype clustering have been highly effective for predicting the propensity of a breast tumor to metastasize with poor patient outcome. Based on hierarchical clustering analyses, breast tumors have been classified into distinct subtypes (basal-like-A and B; ErbB2+; normal breast-like; and luminal A, B and C) (Sorlie *et al.*, 2003; Hennessy *et al.*, 2009). Patients with basal-type tumors lacking estrogen receptor (ER), progesterone receptor and ErbB2—referred to as basal triple-negative breast cancer (BTNBC)—have a worse prognosis compared with patients with more differentiated, less metastatic tumors expressing markers of the luminal lineage, including the transcription factors GATA3 and ER (Perou *et al.*, 2000; Sorlie *et al.*, 2003; Neve *et al.*, 2006). These observations suggest that the constellation of genes responsible for the specification of the luminal or basal subtype of breast cancer may also promote or inhibit metastatic potential. Although gene signatures have been invaluable for defining categories of breast cancer metastatic propensity and patient outcome (van de Vijver *et al.*, 2002; van't Veer *et al.*, 2002; Wang *et al.*, 2005), elucidating the molecular mechanisms governing metastatic propensity remains a critical challenge.

Human breast cancer cell lines recapitulate many important molecular features of breast cancer and have been classified into three of the major tumor subtypes—luminal, basal-A and basal-B—based on microarray analyses (Neve *et al.*, 2006). Breast cancer cell lines clustering within the luminal subtype, such as BT474, show limited invasive properties compared with cell lines of the basal subtype, including the MDA-MB-231 (MB231) cell line, which clusters within the basal-B subtype (Neve *et al.*, 2006). As the MB231 cell line shows many critical biological and molecular features of BTNBC, it has been extensively used as an important model to study this form of breast cancer.

While distinct subtypes of breast cancer have been delineated, few studies have explored whether a

potential plasticity exists for tumor cells of one subtype to trans-differentiate into another subtype and what factors would lead to such a phenotypic shift. Previous studies have demonstrated that overexpression of the mammary luminal transcription factor GATA3 in BTNBC cells could reduce tumorigenicity and metastases. However, no mechanism has been reported that accounts for how GATA3 expression reduces the metastatic propensity of BTNBC cells *in vivo*. In this study, we have determined that suppression of lysyl oxidase (LOX) expression by GATA3 is a major mechanism for the reduction of metastases.

Expression of GATA3 is intimately associated with the luminal subtype of breast cancer and its expression is highly correlated with ER expression and many genes associated with the luminal subtype (Perou *et al.*, 2000; Sorlie *et al.*, 2003; Usary *et al.*, 2004). GATA3 is generally absent or minimally expressed in basal subtypes of breast cancer, including MB231 cells. Recently, GATA3 was shown to be essential for normal mammary gland development and luminal cell differentiation (Kouros-Mehr *et al.*, 2006a; Asselin-Labat *et al.*, 2007). Conditional knockout of GATA3 in mammary epithelial cells resulted in abnormal mammary duct formation (Kouros-Mehr *et al.*, 2006a; Asselin-Labat *et al.*, 2007). Retroviral expression of GATA3 in mammary progenitor cells or in late carcinomas induced the expression of luminal differentiation markers (Asselin-Labat *et al.*, 2007; Kouros-Mehr *et al.*, 2008). Thus, GATA3 appears to be a key factor in determining the biological characteristics of mammary luminal epithelial cells and breast cancers with a luminal phenotype.

In this study, we demonstrate through gene expression profiling that GATA3 induces numerous transcriptional alterations affecting differentiation, metastasis, interactions with the extracellular matrix (ECM) and paracrine signaling. Further, we determined that GATA3 reduces the expression of many metastasis-related genes, including macrophage colony-stimulating factor (CSF-1), which is a potent chemoattractant for macrophages promoting metastatic progression. Importantly, we demonstrate that repression of LOX expression by GATA3 is a key mechanism for the GATA3-mediated inhibition of metastases. LOX expression in breast cancer has been shown to be associated with reduced overall survival and distant metastasis-free survival in ER-negative patients (Erler *et al.*, 2006). The lack of GATA3 expression resulting in elevated LOX expression in human BTNBC may account for the highly metastatic nature of this form of breast cancer and suggests that LOX is an important target for therapy.

Results

GATA3 reduces MB231 cell proliferation in 3D culture, primary tumor outgrowth and metastases, and alters cell morphology and cytoskeletal organization

GATA3 protein was ectopically expressed in MB231 cells through transduction with lentivirus expressing GATA3 (231-GATA3) (Supplementary Figure 1a). In order to confirm that our MB231 cells containing an empty lentiviral vector (231-Empty) and our 231-GATA3 cells showed similar growth and metastatic characteristics as were previously reported, we determined their growth characteristics both *in vitro* and *in vivo*. We observed no differences in apoptosis by ELISA for cytoplasmic histone-associated DNA fragments between 231-Empty and 231-GATA3 cells (Supplementary Figure 1b). Pulse–chase 5-bromo-2-deoxyuridine labeling revealed that GATA3 overexpression in MB231 did not affect proliferation in two-dimensional cultures (Supplementary Figure 1c) as reported previously (Yan *et al.*, 2010). However, we demonstrate for the first time that in three-dimensional (3D) culture using Cultrex Basement Membrane Extract, 231-GATA3 cells were significantly less proliferative compared with 231-Empty control cells ($P<0.001$; Figure 1a). Thus, differences in the rates of cell proliferation between 231-Emtpy and 231-GATA3 may not necessarily be caused only by intrinsic cellular changes, but appear to also result from GATA3 altering cell interactions with the ECM. In two-dimensional culture, 231-Empty cells maintained a spindle, elongated morphology, whereas 231-GATA3 cells were larger and cuboidal (Supplementary Figure 1d). In 3D culture using Basement Membrane Extract, 231-Empty cells appeared invasive by protruding into the Basement Membrane Extract matrix to form interconnected networks of cells, whereas the 231-GATA3 cells appeared less invasive without extended protrusions and formed more tightly organized, rounded clusters (Figure 1b).

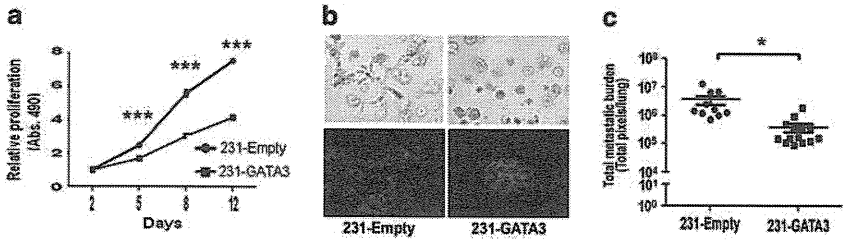

Figure 1 GATA3 overexpression reduces proliferation in 3D culture and experimental metastasis in mice. (**a**) 231-Empty and 231-GATA3 cells were seeded on 3D Cultrex for 12 days. 231-GATA3 cells show reduced proliferation as measured by MTS (mean ± s.e.m., $***P<0.001$). (**b**) Top panels, bright-field images; lower panel, confocal microscopy of cells on 3D Cultrex fixed and stained with DAPI (blue) for nuclear localization and phalloidin (green) for f-actin. (**c**) Lung lesions of mice injected by tail vein with 231-Emtpy and 231-GATA3 cells. Lungs were imaged by fluorescence microscopy, with total metastatic burden calculated per lung ($*P<0.05$).

Similarly, in xenograft studies, primary tumor outgrowth of 231-GATA3 cells was significantly delayed compared with 231-Empty cells when orthotopically transplanted into mammary fat pads (Supplementary Figure 2a), with a concomitant ~40% increase in survival of mice (Supplementary Figure 2b). Histologically, 231-Empty tumors were characterized primarily by spindyloid cells, whereas tumors arising from 231-GATA3 cells appeared primarily epithelioid (Supplementary Figure 2c).

We further confirmed that during early lesion development, tumors arising from 231-GATA3 cells expressed a more differentiated phenotype than tumors from 231-Empty cells. 231-GATA3 tumors were immunoreactive for GATA3, E-cadherin and cytokeratin-8 by immunohistochemistry (IHC) as compared with 231-Empty tumors, which were negative for these markers (Supplementary Figure 2d). Interestingly, there appears to be strong selective pressure against the expression of GATA3 as the tumors grow. Thus, over time, tumors arising from 231-GATA3 cells lose GATA3 expression and the associated changes. Advanced tumors showed similar immunostaining for both Ki-67 and TUNEL in mice receiving either 231-Empty or 231-GATA3 injections (data not shown). Lungs from mice receiving orthotopic implantations of the cells were collected and visualized by immunofluorescence, but we did not observe green fluorescent protein-positive lung lesions at the time when mice were killed because of significant primary tumor burden.

Although we did not observe a statistically significant difference in the number of 231-GATA3 cells as compared with 231-Empty cells invading through Matrigel *in vitro* using the Boyden chamber assay (Supplementary Figure 3a), there was a dramatic increase in the clearing of tail vein-injected 231-GATA3 cells in the lungs compared with 231-Empty cells within the first 24 h following tail vein injection (Supplementary Figure 3b). At 24 h, there was an approximately 75% reduction in the number of 231-GATA3 cells in the lungs compared with the number of cells in the lungs 2 h after injection, whereas at the same time points there was an approximately 20% increase in the number of 231-Empty cells in the lungs (Supplementary Figure 3b). This suggests that GATA3 greatly reduces the ability of MB231 cells to initially survive in the lung metastatic site. Furthermore, mice tail vein-injected with 231-GATA3 cells had a statistically significant ninefold reduction in total metastatic burden in the lung compared with mice injected with the 231-Empty cells 2 months after injection ($P<0.05$; Figure 1c). The observed reduced metastatic burden in the lungs of mice receiving 231-GATA3 cells was the result of a reduced number and smaller size of lesions as observed by immunofluorescence (Supplementary Figure 3c) and by quantitation of hematoxylin and eosin staining (Supplementary Figure 4a) by a pathologist. We previously demonstrated that this method of using immunofluorescence to detect green fluorescent protein-labeled cells in whole lungs by single-cell, whole-organ microscopy is extremely sensitive and quantitative (Barkan *et al.*, 2008).

We additionally quantitated the percentage of lung area occupied by metastatic lesions based on Ki-67 staining by using the Apiro Image Analysis Software. This similarly revealed that GATA3 expression significantly reduced metastatic burden as compared with 231-Empty cells. We further characterized lung lesions from mice 2 months after they received either 231-Empty or 231-GATA3 cells, for proliferation and apoptosis by Ki-67 and TUNEL staining, and observed no statistical differences between these two cohorts (data not shown).

GATA3 profoundly alters the transcriptome of MB231 cells, with a concomitant reduction in the expression of metastasis-associated genes

Gene expression profiling analyses revealed that the expression of 1273 probesets was altered between 231-GATA3 and 231-Empty cells (776 up- and 497 down-regulated in 231-GATA3 cells, with fold change $\geqslant 1.5$ and $P<0.001$, and a false discovery rate of 3% (Supplementary Dataset 1)) and that several biological processes were altered (Supplementary Figure 5).

Microarray analysis further revealed that LOX, a gene functionally involved in cell adhesion, ECM remodeling, migration and metastasis (Erler *et al.*, 2006; Erler *et al.*, 2009), was the gene most down-regulated by GATA3. We investigated whether the dramatic reduction in the metastatic propensity of 231-GATA3 cells was the result of GATA3-dependent inhibition of LOX expression. Quantitative real-time PCR (Q-RT–PCR) confirmed that LOX expression was reduced by 70% in 231-GATA3 cells compared with 231-Empty cells ($P<0.01$; Figure 2a). We further confirmed at the protein level that GATA3 expression resulted in a reduction of LOX expression. 231-Empty and 231-GATA3 cell pellets were analyzed for GATA3 and LOX expression by IHC. Whereas 231-Empty cells were negative for GATA3 expression, LOX expression was clearly demonstrable (Figure 2b). However, most 231-GATA3 cells showed strong nuclear staining for GATA3, but LOX expression was not detectable (Figure 2b). Similarly, early 231-GATA3 primary tumors showed less LOX expression by IHC compared with 231-Empty tumors (Supplementary Figure 2d). Similar analyses were performed on metastatic lesions in the lung. Lung lesions arising from 231-Empty lacked nuclear GATA3 staining by IHC, whereas 231-GATA3 lung lesions showed positive GATA3 staining (Supplementary Figure 6a). Furthermore, lung lesions from 231-Emtpy cells expressed LOX protein by IHC, whereas 231-GATA3 metastatic lesions stained poorly for LOX (Supplementary Figure 7a).

When GATA3 was expressed in another BTNBC cell line, Hs578T, LOX expression was reduced by 30% ($P<0.05$; Figure 2a), further demonstrating that GATA3 could suppress LOX expression. Furthermore, 231-GATA3 cells had significantly reduced LOX catalytic activity compared with 231-Empty cells, consistent with the reduction in LOX expression ($P<0.01$; Figure 2c).

To additionally confirm that GATA3 regulates LOX expression in breast cancer cells, we knocked down

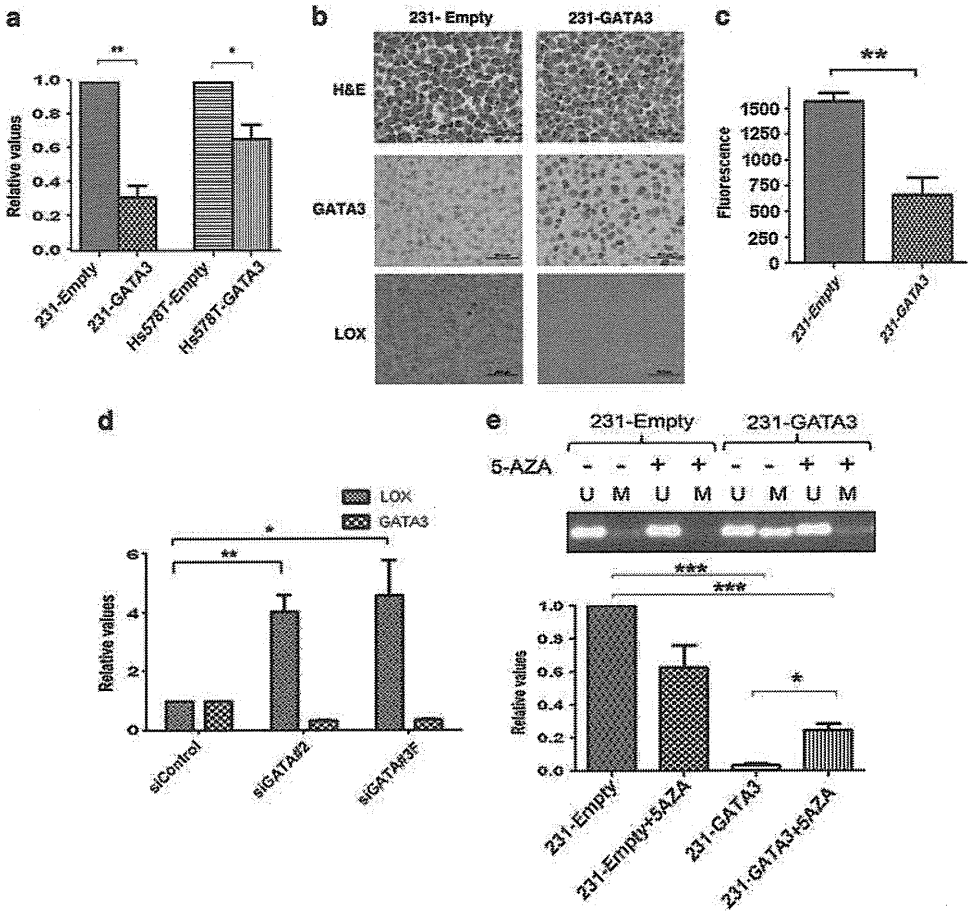

Figure 2 GATA3 regulates LOX expression in breast cancer cells in part through LOX promoter methylation. (**a**) Relative LOX expression by Q-RT–PCR. Samples were normalized to cyclophilin-B. Overexpression of GATA3 in MB231 and Hs578T cells reduces LOX mRNA expression (**$P<0.01$, *$P<0.05$). (**b**) Immunohistochemical staining of cell pellets confirmed positive staining for GATA3 in only 231-GATA3 cells and positive staining for LOX only in 231-Empty cells. (**c**) Relative LOX activity in the medium of 231-Empty and 231-GATA3 cells measured as the increase in fluorescence over β-aminopropionitrile-containing controls. Relative activity measured at 2400 s (40 min, **$P<0.01$). (**d**) Relative LOX and GATA3 mRNA expression measured by Q-RT–PCR. BT474 cells were transfected with GATA3 small interfering RNA for 72 h prior to RNA isolation (*$P<0.05$, **$P<0.01$). (**e**) Cells were treated with 5-AZA for 4 days prior to DNA or mRNA isolation. Top panel: PCR of the LOX promoter using LOX unmethylated (U) or methylated (M) specific primers. Lower panel: Relative LOX expression by Q-RT-PCR. Treatment of 231-GATA3 cells with 5-AZA increased LOX mRNA expression (***$P<0.001$, *$P<0.05$).

GATA3 expression using small interfering RNAs and measured LOX expression. Seventy-five percent knockdown of GATA3 in the luminal, GATA3-positive breast cancer cell line BT474 increased LOX expression over four-fold (confirmed using two different small interfering RNAs) (Figure 2d). These findings suggest that GATA3 can regulate LOX expression in both basal and luminal breast cancer subtypes.

GATA3 inhibits LOX expression through DNA methylation

Methylation of the LOX promoter in 231-GATA3 cells was significantly increased as compared with control cells (Figure 2e). Although treatment with the methylation inhibitor 5-aza-2′-deoxycytidine (5-AZA) diminished the promoter methylation of LOX in 231-GATA3 cells to levels similar to that in 231-Empty cells, LOX expression measured by Q-RT–PCR in 231-GATA3 cells treated with 5-AZA was not completely restored to levels observed in 231-Empty cells treated with 5-AZA (Figure 2e), suggesting that GATA3 also regulates LOX expression through methylation-independent pathways. Although there was a trend for reduced LOX expression in 231-Empty cells using 5-AZA treatment as compared with vehicle, these differences were not statistically significant and may have arisen from some toxicity effects of the drug during the 4-day treatment period. We observed no changes in GATA3 expression using 5-AZA treatment in 231-Empty cells (data not shown).

GATA3 reduces macrophage recruitment to metastatic lesions and CSF-1 expression

As myeloid cell recruitment has been shown to be an important component of metastatic progression especially in the promotion of metastases by LOX, we investigated whether GATA3 expression was also associated with changes in cytokine expression related to myeloid recruitment. Our microarray analysis identified

an almost twofold reduction of CSF-1 expression (a key chemokine that recruits macrophages) in 231-GATA3 cells as compared with control cells (see below). This was confirmed by ELISA showing a 40% reduction in secreted CSF-1 by 231-GATA3 as compared with 231-Empty cells ($P<0.001$; Figure 3a). Reduced secretion of granulocyte–macrophage CSF in 231-GATA3 cells ($P<0.01$) was also observed, although total levels were lower compared with those of CSF-1. There was no change in the secreted macrophage migration-inhibitory factor (Figure 3a).

As we observed a reduction in secreted CSF-1 in 231-GATA3 cells as compared with 231-Empty cells, and macrophages have been shown to be an important component of the metastatic process (Condeelis and Pollard, 2006), we quantitated macrophage recruitment in the lungs of mice injected with 231-Empty or 231-GATA3 cells by flow cytometry. Lungs from mice tail vein-injected with 231-GATA3 cells were infiltrated with about 50% fewer mature tumor-associated macrophages (F4/80+/Gr-1−) as compared with the lungs of mice receiving 231-Empty cells (53% F4/80+/Gr-1− cells for 231-Empty versus 29% for 231-GATA3; $P<0.05$; Figure 3b). There was no change in the percent of CD11b+/Gr-1+ immune cells recruited (Figure 3b).

GATA3 increases the pattern of luminal cell type gene expression

Using a previously identified gene signature that categorizes the human breast cancer cells into luminal, basal-A or basal-B subtypes (Neve *et al.*, 2006), we combined our microarray data with data from the 51 breast cancer cell line data set of Neve *et al.* to perform hierarchical clustering of all of the cell lines by using 249 unique signature genes available from both platforms (see Supplementary Materials and methods). 231-Empty cells, as expected, clustered within the highly invasive basal-B subtype, whereas the 231-GATA3 cells clustered within the luminal subtype (Supplementary Figure 8a). GATA3 reduced the expression of 76 named genes associated with the basal phenotype and increased the expression of 46 named genes associated with the luminal phenotype (Supplementary Dataset 2). Among the genes upregulated by GATA3 expression were members of the claudin family, claudin-3 and claudin-4, whose low expression is characteristic of the claudin-low subtype of breast cancer (Hennessy *et al.*, 2009). Q-RT–PCR confirmed that GATA3 altered the expression of several signature genes that distinguish the luminal, basal-A and basal-B phenotypes toward the luminal phenotype (ANK3, CLDN3, CLDN4, KRT19, EPCAM, TSPAN13, ERBB3, FSCN1 and HMGA2) (Supplementary Figure 8b). Western blot confirmed increased expression of cytokeratin-18 and re-expression of E-cadherin in 231-GATA3 cells (Supplementary Figure 8c).

LOX and GATA3 are inversely expressed in breast cancer cells

To address whether LOX and GATA3 expression in breast cancers may be inversely associated, we performed a retrospective analysis of the previously published microarray data for 51 breast cancer cell lines (Neve *et al.*, 2006). GATA3 expression is inversely associated with LOX expression ($P<0.001$; Figures 4a and b), with the luminal subtype cell lines expressing high GATA3 and low LOX, whereas LOX expression was high in the more invasive basal subtypes (basal-B > basal-A) lacking GATA3 expression (Figure 4c).

Re-expression of LOX in 231-GATA3 cells reverses metastatic propensity

231-GATA3 cells were transduced with lentiviral vectors expressing control red fluorescent protein (RFP) (231-GATA3-Empty), or both LOX and RFP (231-GATA3-LOX), and examined for their metastatic potential *in vivo*. Overexpression of LOX in 231-GATA3 cells was confirmed by Q-RT–PCR (Figure 5a). LOX protein levels were increased in 231-GATA3-LOX cells as compared with 231-GATA3-Empty cells as determined by IHC (Figure 5b). Similarly, LOX activity was increased in 231-GATA3-LOX cells as compared with 231-GATA3-Empty cells (Figure 5c). However, 231-GATA3-LOX cells maintained their cuboidal morphology and continued to express E-cadherin (Supplementary Figures 9a and b).

We observed no differences in the rates of proliferation in two-dimensional or 3D culture, or in invasive potential by Boyden chamber invasion assay, between 231-GATA3-Empty and 231-GATA3-LOX *in vitro* (data not shown). Most importantly, single-cell, whole-organ microscopy analysis revealed that mice tail vein-injected with 231-GATA3-LOX cells showed a statistically significant marked increase in total lung

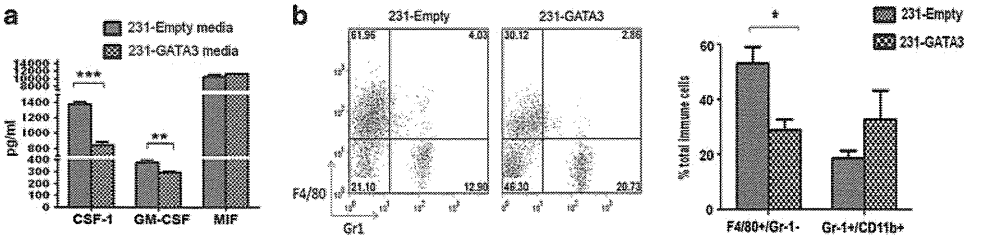

Figure 3 GATA3 reduces macrophage recruitment to the lung (**a**) ELISA of medium collected from 231-Empty and 231-GATA3 cells. 231-GATA3 cells showed reduced secretion of CSF-1 and granulocyte–macrophage-CSF (***$P<0.001$, **$P<0.01$). (**b**) Flow-cytometric analyses of immune cells collected from the lungs of tail vein-injected mice ($n=4$). Cells were labeled with anti-CD45, F4/80, Gr-1 or CD11b antibodies. Lungs collected from mice injected with 231-GATA3 cells showed reduced F4/80+/Gr-1− recruitment (*$P<0.05$).

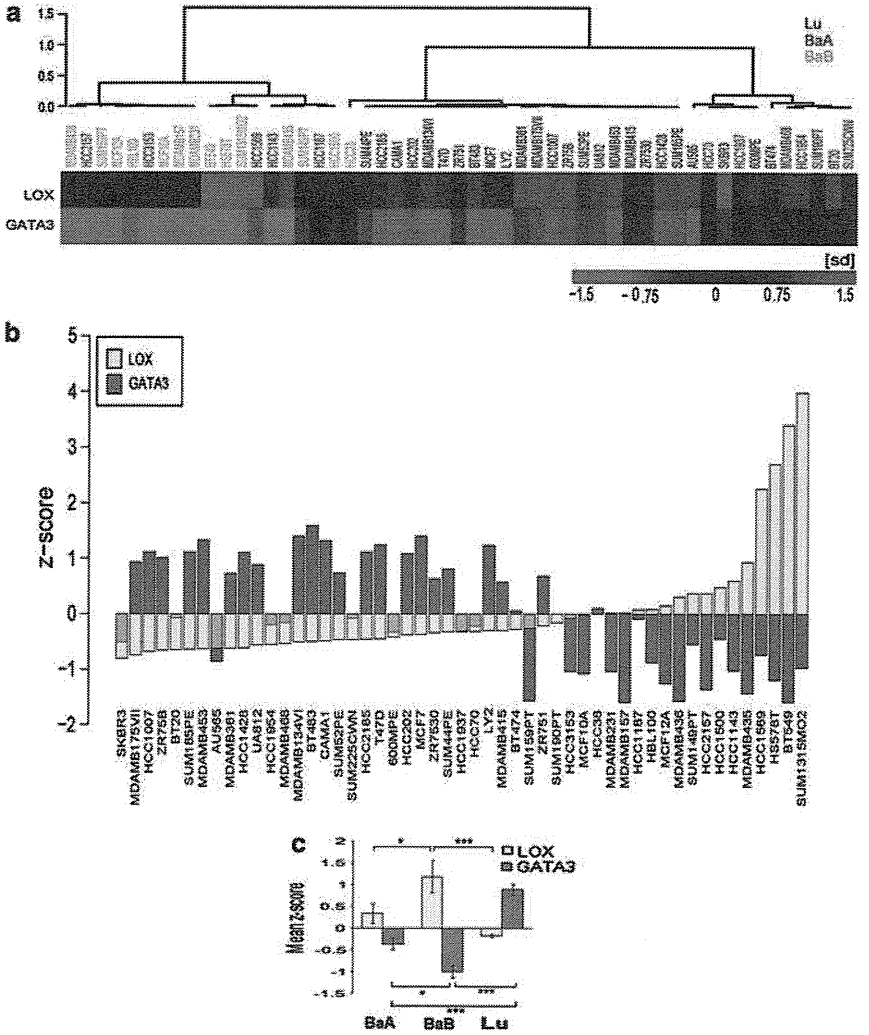

Figure 4 Analysis of the Neve *et al.* 51 breast cancer cell line microarray database for LOX and GATA expression (Neve *et al.*, 2006). (**a**) Heat-map of LOX and GATA3 expression in breast cancer cell lines. The displayed expression of each gene was standardized using *Z*-score. The hierarchical clustering used 1-uncentered correlation distance metric and average linkage. (**b**) Relative GATA3 and LOX expression in breast cancer cell lines arranged in order of increasing LOX expression (Pearson's correlation coefficient $r=-0.53$, $P<0.001$). (**c**) Relative expression of GATA3 as represented by *Z*-score (see Supplementary Materials and methods). GATA3 is enriched in luminal breast cancer cells, whereas LOX is enriched in basal-B cells ($*P<0.05$, $***P<0.001$).

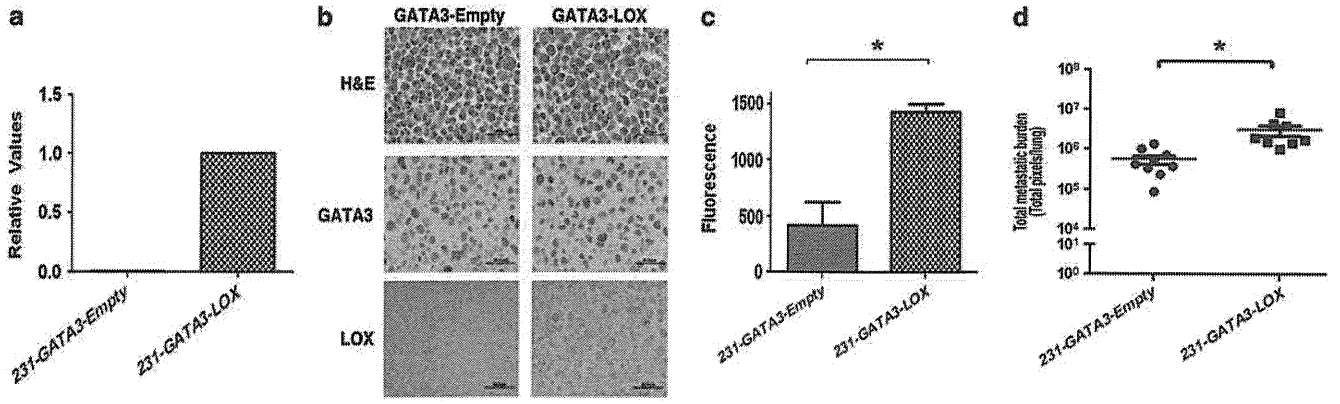

Figure 5 Re-expression of LOX in 231-GATA3 cells increased the metastatic potential of 231-GATA3 cells. (**a**) Lentiviral transduction of 231-GATA3 cells with LOX increases LOX expression in 231-GATA3 cells. Relative LOX expression by Q-RT–PCR. (**b**) Immunohistochemical staining of cell pellets confirmed positive staining for GATA3 in 231-GATA3-Empty and 231-GATA3-LOX cells, and positive staining for LOX in only 231-GATA3-LOX cells. (**c**) Relative LOX enzymatic activity measured at 2400 s (40 min, $*P<0.05$). (**d**) Mice tail-vein-injected with 231-GATA3-Empty and 231-GATA3-LOX cells, with lungs collected after 2 months. Lungs imaged by fluorescence microscopy, with total metastatic burden calculated per lung ($*P<0.05$).

metastatic burden of more than five-fold compared with 231-GATA3-Empty cells ($P<0.05$; Figure 5d) that was similar to that of 231-Empty cells (Figure 1c). This was further validated by image quantitation of Ki-67 expression and hematoxylin and eosin staining of metastatic lung lesions using the Apirio Image Analysis software (Supplementary Figure 4b), which demonstrated an approximately eightfold increase in metastatic burden owing to increased size and number of lesions in 231-GATA3-LOX cells as compared with 231-GATA3-Empty cells. Importantly, this demonstrates that the reduction in metastatic potential of tumor cells by the suppression of LOX by GATA3 can be restored by the re-expression of LOX.

There was a selection against GATA3 as the metastatic lesions progressed, consistent with our model that GATA3 reduces metastatic potential. GATA3 expression was still detected in some of the lung metastatic lesions from both 231-GATA3-Empty and 231-GATA3-LOX cells (Supplementary Figure 6b). Metastatic lung lesions from 231-GATA3-Empty cells showed minimal LOX expression, whereas metastatic 231-GATA3-LOX lesions showed strong LOX expression by IHC (Supplementary Figure 7b).

We determined that the great majority of genes whose expression was initially altered by GATA3 were not affected by re-expression of LOX in MB231. In fact, only nine named genes dysregulated by GATA3 were expressed in the opposite direction by re-expression of LOX (adrenomedullin, fibronectin, MMP1, MMP12, anterior gradient homolog-2, IL7R, neural precursor cell expressed–developmentally downregulated 4-like, RNA-binding protein with multiple splicing and chordin-like-1). Thus, the effect of LOX appears to be more specific for promoting a more metastatic phenotype than globally affecting the transcriptome.

As in the previous tail vein injection experiment, we observed no lung metastasis by immunofluorescence in mice receiving orthotopic implantations of 231-GATA3-Empty versus 231-GATA3-LOX cells.

Patients expressing a high LOX/GATA3 ratio have poor prognosis

Retrospective statistical analyses of the NKI patient microarray database ($n=295$) (van de Vijver *et al.*, 2002) revealed higher LOX expression in the basal subtype of breast cancer as compared with the luminal-A ($P<0.001$) and luminal-B types ($P<0.01$), whereas GATA3 was lower in the basal subtype compared with luminal-A ($P<0.001$) and the luminal-B ($P<0.001$) (Figure 6a). Importantly, an inverse correlation between LOX and GATA3 expression was also demonstrated across the breast cancer subtypes ($r=-0.3$; $P<0.001$; Figure 6b), consistent with our results for the 51 breast cancer cell lines. Although we observed an inverse association between GATA3 and LOX expression in patients, there were some tumors expressing relatively high or low levels of both GATA3 and LOX. Therefore, additional factors may be involved in regulating the expression of LOX in breast cancer patients. These

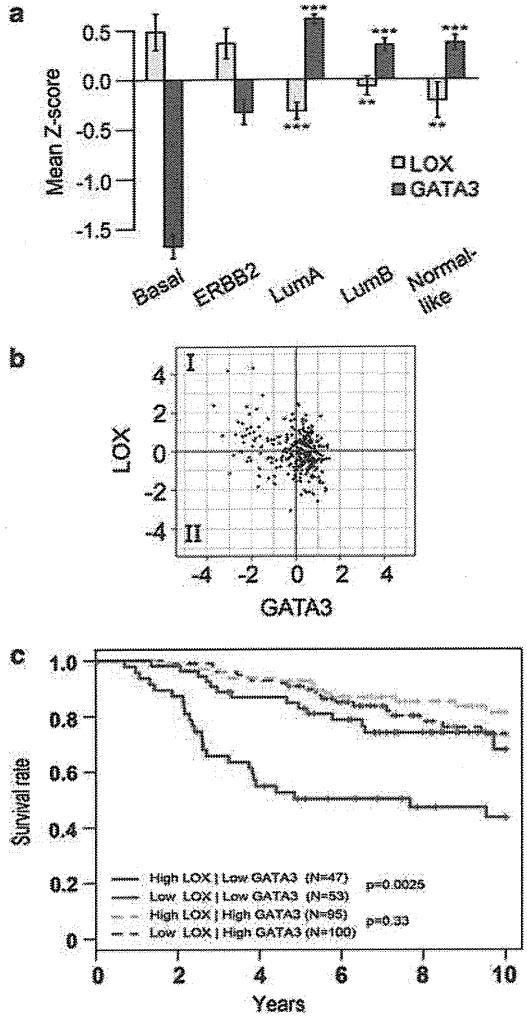

Figure 6 Retrospective microarray analysis of breast cancer patient microarray data from van de Vijver *et al.* (2002). (**a**) GATA3 is associated with the luminal-A and luminal-B subtype, whereas LOX is enriched in the basal subtype (***$P<0.001$, **$P<0.01$). (**b**) Correlation between LOX (y-axis) and GATA3 (x-axis) among breast cancer patients ($n=295$). GATA3 and LOX are inversely correlated (Pearson's correlation coefficient $r=-0.30$, $P<0.001$). (**c**) Kaplan–Meier survival curves showing that patients with high LOX and reduced GATA3 expression (quadrant I in panel **b** above) had significantly reduced overall survival (hazard ratio = 2.65, $P<0.01$) compared with patients with low LOX and Low GATA3 (quadrant II in panel **b** above). High and low are defined as above or below median expression as depicted in panel **b**. Log-rank test P-values are indicated. The interaction between LOX and GATA3 was statistically significant ($P<0.05$).

retrospective data along with our breast cancer cell line data support a model whereby breast cancers that express low GATA3 (clustering with the basal subtype) and elevated LOX have an increased metastatic potential. GATA3 expression (and possibly ER expression) in luminal tumors appears to override the survival effects of high LOX expression. A large portion of basal ER-negative tumors that express very low levels of GATA3 express high levels of LOX. Kaplan–Meier analysis using the above database revealed that patients that show a low GATA3/high LOX expression pattern have significantly reduced survival compared with

patients with a low GATA3/low LOX expression pattern ($P<0.01$; Figure 6c). Thus, LOX may serve as a predictor of survival in patients with low GATA3 expression. Even in cases where tumors expressed high levels of LOX, the concomitant expression of GATA3 was shown to improve survival (Figure 6c); thus GATA3 expression may have a dominant protective role to prolong survival that overcomes high LOX expression through other mechanisms.

Discussion

This study has identified a key mechanism for the GATA3-induced inhibition of the metastatic propensity of BTNBC, an aggressive form of breast cancer with poor prognosis. We have demonstrated that expression of GATA3 induces global changes to the transcriptome associated with a significant reduction in metastatic propensity and extended survival of mice in xenograft studies. While GATA3 has previously been shown to reduce the metastases of MB231 cells (Dydensborg *et al.*, 2009; Yan *et al.*, 2010), this study identified a major mechanism for the GATA3-induced inhibition of metastases through downregulation of LOX. GATA3 has been shown to be a key developmental transcription factor in the hematological system and during mammary luminal epithelial cell development (Zhou and Ouyang, 2003; Kouros-Mehr *et al.*, 2006a; Kouros-Mehr and Werb, 2006b). Expression of GATA3 is a defining property of luminal-type breast cancers, whereas it is minimally expressed in basal-type breast cancers.

We observed that many genes that have been shown previously to be involved in metastatic progression were coordinately downregulated by GATA3, including Fascin homolog-1 (FSCN1), chemokine receptor-4 (CXCR4), mannosidase, alpha, class-1A, member-1 (MAN1A1), tenascin-C and CSF-1. These genes were previously identified to be part of a lung metastasis signature in MB231 cells (Minn *et al.*, 2005), suggesting that expression of GATA3 in BTNBC cells inhibits the expression of genes that promote invasion and dissemination. Although GATA3 was previously shown to reduce the metastatic potential of MB231 or the MB231 variant LM2-4175 cell line that is highly metastatic to the lung in mice (Dydensborg *et al.*, 2009; Yan *et al.*, 2010), the factor(s) responsible for the marked reduction of metastases *in vivo* was not identified. Neither study found and confirmed an *in vivo* mechanism through which GATA3 overexpression inhibits metastases as presented in our study. We demonstrate for the first time that repression of LOX by GATA3 is a major mechanism resulting in the inhibition of metastases, and that re-establishment of LOX expression in the 231-GATA3 cells restored the metastatic phenotype.

Several mechanisms may be involved through which LOX affects metastases. Intracellular active LOX facilitates migration and invasiveness in breast cancer cells through a hydrogen peroxide-mediated mechanism that results in the phosphorylation and activation of Src/focal adhesion kinase (FAK) pathways (Payne *et al.*, 2005). Activated LOX secreted into the extracellular environment has an important role in potentiating metastatic tumor cell growth through cross-linking of several collagen types and elastins in the ECM (Kagan and Li, 2003; Payne *et al.*, 2007; Erler *et al.*, 2009; Levental *et al.*, 2009). Most importantly, inhibition of LOX enzymatic activity in orthotopically implanted MB231 cells eliminates lung metastases (Erler *et al.*, 2006; Bondareva *et al.*, 2009). More recently, LOX was found to also activate FAK and promote invasiveness in an integrin-β1-dependent mechanism involving collagen cross-linking and tissue stiffening (Levental *et al.*, 2009).

We also observed that, whereas overexpression of LOX significantly increased lung metastasis by tail vein injection of 231-GATA3 cells, there was a paradoxical reduction in primary tumor outgrowth. This is consistent with another study where overexpression of LOX in the gastric cancer cell line, MKN28, reduced primary tumor growth in a xenograft model (Kaneda *et al.*, 2004). Treatment of MB231 xenografts with β-aminopropionitrile, shLOX or an inhibitory LOX antibody reduced metastasis to the lung but did not affect primary tumor growth (Erler *et al.*, 2006), whereas inhibition of LOX catalytic activity in uveal melanoma significantly reduced cellular invasion (Abourbih *et al.*, 2010). The mechanisms responsible for these differences in response to LOX expression between the primary and metastatic sites remain unknown, but may be attributed to the dual role of LOX as a tumor suppressor and as a tumor promoter. The function of LOX is likely dependent on the cellular context (Payne *et al.*, 2007), the biological activity of its propeptide (Palamakumbura *et al.*, 2009; Grimsby *et al.*, 2010) and perhaps the metastatic site. Although we have only studied the effect of GATA3 and LOX in the lung, LOX might also affect metastasis at other organs.

LOX is inactivated by methylation in human gastric cancer and methylation status was associated with loss of LOX mRNA expression in gastric cancers (Kaneda *et al.*, 2004). However, mechanisms responsible for LOX methylation are still unknown. Here, we provide evidence implicating changes in the DNA methylation status of the LOX promoter to be partially responsible for the reduced expression of LOX upon overexpression of GATA3. Preliminary analyses of the genome-wide methylation patterns by microarray indicates that regions in the 5′ regulatory region and first exon indicate a significant increase in methylation in the 231-GATA3 cells as compared with Empty cells. These results will require further validation and functional analyses to more precisely define the role of methylation in regulating LOX expression.

Although our studies demonstrated that GATA3 alone is sufficient to reduce LOX expression through changes in methylation, which may be direct or indirect, future studies are required to gain further insights into the underlying mechanism that results in the methylation of the LOX promoter and subsequent suppression of LOX expression. It is also likely that in addition to its

effect on methylation, GATA3 alters the expression of other genes that positively or negatively regulate the transcription of LOX or its post-translational stability. Chip-on-Chip studies did not identify GATA3-binding sites in the LOX promoter, suggesting that GATA3 does not directly bind to and inhibit the LOX promoter (Paul Meltzer, personal communication). Whereas LOX showed increased methylation resulting in reduced expression, E-cadherin showed reduced methylation at the DNA promoter upon GATA3 overexpression (data not shown). Therefore, the GATA3-dependent changes in the epigenome appear to be gene-specific.

Our results suggest that expression of GATA3 in the mammary gland may promote global changes in gene expression, resulting in the expression of genes involved in luminal differentiation, and in the repression of genes associated with the basal subtype through epigenetic modifications such as alterations in methylation patterns. We demonstrated increased LOX expression associated with the more invasive basal-B subtype in breast cancer cell lines and with the basal subtype in breast cancer patients who have a poorer overall survival as compared with patients with the luminal-A subtype (van de Vijver *et al.*, 2002). Although GATA3 can regulate LOX expression, GATA3 may not be the only factor that regulates LOX expression. In addition to LOX, basal-B cells likely have additional factors that could contribute to metastasis. Most importantly, our retrospective analysis revealed that LOX expression is critical at predicting survival in patients with reduced GATA3 expression.

Expression of GATA3 in MB231 cells also resulted in important changes in how the cells interacted with the ECM. Many genes altered by GATA3 expression are extracellular or plasma membrane proteins, which may be responsible for the observed reduced proliferation of 231-GATA3 cells in 3D cultures and their more organized compacted spherical structure in 3D cultures as compared with 231-Empty cells.

Additionally, expression of GATA3 led to changes in the transcription of genes that induce important paracrine effects in the stroma. Recruitment of macrophages at the metastatic site has been shown to be a critical component for metastatic growth (Condeelis and Pollard, 2006). CSF-1 secretion was significantly reduced in 231-GATA3 cells as compared to 231-Empty cells, which may be responsible for our observed reduction in macrophage infiltration into the lungs of 231-GATA3 tail vein-injected mice as compared with 231-Empty. In addition, we observed dramatically increased clearing of tumor cells in the lung within the first 24 h of tail vein injection of 231-GATA3 cells as compared with control cells, suggesting that GATA3 may reduce the ability of cells to survive during early stages of tumor infiltration at the metastatic site. It is also possible that expression of GATA3 may inhibit additional paracrine factors required for recruitment of macrophages. Taken together, our data suggest that GATA3 alone is sufficient to alter molecular events that can regulate metastasis.

It is, therefore, conceivable that tissue- or subtype-specific transcription factors responsible for promoting global changes in the tumor transcriptome may be critical targets that account for the heterogeneous nature of tumors; predict patient outcome and most importantly, may become valuable novel therapeutic targets. The data presented here provide strong evidence indicating that induced expression of GATA3 or inhibition of LOX activity may be worthy therapeutic approaches for the reduction of metastasis in breast cancer.

Materials and methods

Cell lines, transfection and lentiviral infection
MB231, BT474 and Hs578T cells were obtained from American Tissue Culture Collection (ATCC, Manassas, VA, USA). Cells were negative for mycoplasma. See Supplementary Materials and methods for experimental details.

Methylation-specific PCR
Cells were treated with vehicle or 5-AZA (Sigma, St Louis, MO, USA) for 4 days prior to DNA isolation. Details of methylation-specific PCR are provided in the Supplementary Materials and methods.

Mice, necropsy and ex vivo *imaging*
All animal work was performed in accordance with the guidelines of the Animal Care and Use of Laboratory Animals (NIH publication no. 86-23, 1985) under an approved animal protocol. Xenograft studies were performed by using 6- to 8-week-old female SCID or NOD/SCID mice (NCI, Frederick, MD, USA or Jackson Laboratories, Bar Harbor, ME, USA). Details of animal work are provided in the Supplementary Materials and methods.

LOX activity
LOX activity was measured as the fluorometric β-aminopropionitrile-inhibitable LOX activity assay by using Amplex red (Palamakumbura and Trackman, 2002). See Supplementary Materials and methods for a detailed description.

Immunoblotting and antibodies
Cells were lysed in ice-cold radioimmunoprecipitation assay buffer for western blot analyses as described previously (Hoenerhoff *et al.*, 2009). GATA3 (Santa Cruz Biotechnology, Santa Cruz, CA, USA) and β-actin (Sigma) antibodies were used.

3D culture and proliferation assay
Cells were cultured in growth factor-reduced 3D Cultrex Basement Membrane Extract (Trevigen, Gaithersburg, MD, USA) as described previously, with minor modifications (Barkan *et al.*, 2008, 2010). Cells were cultured in complete medium and medium was replenished every 2 days. Proliferation was measured as described previously by Barkan *et al.* (2008) at 2, 5, 8 and 12 days after seeding by CellTiter 96 AQueous Non-Radioactive Cell Proliferation Assay (MTS) (Promega, Madison, WI, USA).

Immunofluorescence and confocal microscopy
Cells grown in 3D culture were imaged by confocal microscopy as described previously (Barkan *et al.*, 2008). Briefly, cells were cultured in eight-well chamber glass slides pre-coated with Cultrex. For f-actin staining, cells were incubated overnight with Alexa-Fluor-488 phalloidin (Molecular Probes, Eugene, OR, USA) and mounted with VECTASHIELD Mounting

Medium with 4′-6-diamidino-2-phenylindole (DAPI) (Vector Laboratories, Burlingame, CA, USA). The slides were imaged using a Leica confocal microscope (Leica Microsystems AG, Buffalo Grove, IL, USA).

Flow-cytometric analysis
Cell-cycle profiles were assayed by 5-bromo-2-deoxyuridine pulse labeling and flow-cytometric analysis were performed as described previously (Chu *et al.*, 2005). For myeloid analysis, mice were tail-vein-injected with one million cells and lungs were harvested after 2 months. See Supplementary Materials and methods for experimental details.

Microarray data processing
Total RNA was isolated by Trizol (Invitrogen, Carlsbad, CA, USA) from 231-Empty and 231-GATA3 cells for microarray analysis. See Supplementary Material and methods for detailed descriptions. Data have been deposited in GEO (reviewer access only: URL http://www.ncbi.nlm.nih.gov/projects/geo/query/acc.cgi?acc = GSE24249).

Conflict of interest

The authors declare no conflict of interest.

Acknowledgements

We thank Drs Lalage Wakefield and Li Yang for helpful scientific discussions. We also thank Lara El-Touny, Dalit Barkan, Zi-Yao Liu, TingHu Qiu, Anthony Vieira, Christina Bennett, Christine Tomlinson, Steven Austin, Christian Mustroph and Wei-Chu Lai for technical assistance; Paul Meltzer for sharing unpublished data; the LRBGE Fluorescence Imaging Core and Chand Khanna for the use of fluorescence microscopy equipment; and Julie Foley and Norris Flagler for technical assistance with image analysis. This research was supported in part by the Intramural Research Program, Center for Cancer Research, NCI, NIH. IMC acknowledges support from the Department of Defense Breast Cancer Research Program (W81XWH-10-2-0030).

References

Abourbih DA, Di CS, Orellana ME, Antecka E, Martins C, Petruccelli LA *et al.* (2010). Lysyl oxidase expression and inhibition in uveal melanoma. *Melanoma Res* **20**: 97–106.

Asselin-Labat ML, Sutherland KD, Barker H, Thomas R, Shackleton M, Forrest NC *et al.* (2007). Gata-3 is an essential regulator of mammary-gland morphogenesis and luminal-cell differentiation. *Nat Cell Biol* **9**: 201–209.

Barkan D, El Touny LH, Michalowski AM, Smith JA, Chu I, Davis AS *et al.* (2010). Metastatic growth from dormant cells induced by a col-I-enriched fibrotic environment. *Cancer Res* **70**: 5706–5716.

Barkan D, Kleinman H, Simmons JL, Asmussen H, Kamaraju AK, Hoenorhoff MJ *et al.* (2008). Inhibition of metastatic outgrowth from single dormant tumor cells by targeting the cytoskeleton. *Cancer Res* **68**: 6241–6250.

Bondareva A, Downey CM, Ayres F, Liu W, Boyd SK, Hallgrimsson B *et al.* (2009). The lysyl oxidase inhibitor, beta-aminopropionitrile, diminishes the metastatic colonization potential of circulating breast cancer cells. *PLoS One* **4**: e5620–e562.

Chu I, Blackwell K, Chen S, Slingerland J. (2005). The dual ErbB1/ErbB2 inhibitor, lapatinib (GW572016), cooperates with tamoxifen to inhibit both cell proliferation- and estrogen-dependent gene expression in antiestrogen-resistant breast cancer. *Cancer Res* **65**: 18–25.

Condeelis J, Pollard JW. (2006). Macrophages: obligate partners for tumor cell migration, invasion, and metastasis. *Cell* **124**: 263–266.

Dydensborg AB, Rose AA, Wilson BJ, Grote D, Paquet M, Giguere V *et al.* (2009). GATA3 inhibits breast cancer growth and pulmonary breast cancer metastasis. *Oncogene* **28**: 2634–2642.

Erler JT, Bennewith KL, Cox TR, Lang G, Bird D, Koong A *et al.* (2009). Hypoxia-induced lysyl oxidase is a critical mediator of bone marrow cell recruitment to form the premetastatic niche. *Cancer Cell* **15**: 35–44.

Erler JT, Bennewith KL, Nicolau M, Dornhofer N, Kong C, Le QT *et al.* (2006). Lysyl oxidase is essential for hypoxia-induced metastasis. *Nature* **440**: 1222–1226.

Grimsby JL, Lucero HA, Trackman PC, Ravid K, Kagan HM. (2010). Role of lysyl oxidase propeptide in secretion and enzyme activity. *J Cell Biochem* **111**: 1231–1243.

Gupta GP, Massague J. (2006). Cancer metastasis: building a framework. *Cell* **127**: 679–695.

Hennessy BT, Gonzalez-Angulo AM, Stemke-Hale K, Gilcrease MZ, Krishnamurthy S, Lee JS *et al.* (2009). Characterization of a naturally occurring breast cancer subset enriched in epithelial-to-mesenchymal transition and stem cell characteristics. *Cancer Res* **69**: 4116–4124.

Hoenerhoff MJ, Chu I, Barkan D, Liu ZY, Datta S, Dimri GP *et al.* (2009). BMI1 cooperates with H-RAS to induce an aggressive breast cancer phenotype with brain metastases. *Oncogene* **28**: 3022–3032.

Kagan HM, Li W. (2003). Lysyl oxidase: properties, specificity, and biological roles inside and outside of the cell. *J Cell Biochem* **88**: 660–672.

Kaneda A, Wakazono K, Tsukamoto T, Watanabe N, Yagi Y, Tatematsu M *et al.* (2004). Lysyl oxidase is a tumor suppressor gene inactivated by methylation and loss of heterozygosity in human gastric cancers. *Cancer Res* **64**: 6410–6415.

Kouros-Mehr H, Bechis SK, Slorach EM, Littlepage LE, Egeblad M, Ewald AJ *et al.* (2008). GATA-3 links tumor differentiation and dissemination in a luminal breast cancer model. *Cancer Cell* **13**: 141–152.

Kouros-Mehr H, Slorach EM, Sternlicht MD, Werb Z. (2006a). GATA-3 maintains the differentiation of the luminal cell fate in the mammary gland. *Cell* **127**: 1041–1055.

Kouros-Mehr H, Werb Z. (2006b). Candidate regulators of mammary branching morphogenesis identified by genome-wide transcript analysis. *Dev Dyn* **235**: 3404–3412.

Levental KR, Yu H, Kass L, Lakins JN, Egeblad M, Erler JT *et al.* (2009). Matrix crosslinking forces tumor progression by enhancing integrin signaling. *Cell* **139**: 891–906.

Minn AJ, Gupta GP, Siegel PM, Bos PD, Shu W, Giri DD *et al.* (2005). Genes that mediate breast cancer metastasis to lung. *Nature* **436**: 518–524.

Neve RM, Chin K, Fridlyand J, Yeh J, Baehner FL, Fevr T *et al.* (2006). A collection of breast cancer cell lines for the study of functionally distinct cancer subtypes. *Cancer Cell* **10**: 515–527.

Palamakumbura AH, Trackman PC. (2002). A fluorometric assay for detection of lysyl oxidase enzyme activity in biological samples. *Anal Biochem* **300**: 245–251.

Palamakumbura AH, Vora SR, Nugent MA, Kirsch KH, Sonenshein GE, Trackman PC. (2009). Lysyl oxidase propeptide inhibits prostate cancer cell growth by mechanisms that target FGF-2-cell binding and signaling. *Oncogene* **28**: 3390–3400.

Payne SL, Fogelgren B, Hess AR, Seftor EA, Wiley EL, Fong SF *et al.* (2005). Lysyl oxidase regulates breast cancer cell migration and

adhesion through a hydrogen peroxide-mediated mechanism. *Cancer Res* **65**: 11429–11436.
Payne SL, Hendrix MJ, Kirschmann DA. (2007). Paradoxical roles for lysyl oxidases in cancer—a prospect. *J Cell Biochem* **101**: 1338–1354.
Perou CM, Sorlie T, Eisen MB, van de RM, Jeffrey SS, Rees CA *et al.* (2000). Molecular portraits of human breast tumours. *Nature* **406**: 747–752.
Sorlie T, Tibshirani R, Parker J, Hastie T, Marron JS, Nobel A *et al.* (2003). Repeated observation of breast tumor subtypes in independent gene expression data sets. *Proc Natl Acad Sci USA* **100**: 8418–8423.
Usary J, Llaca V, Karaca G, Presswala S, Karaca M, He X *et al.* (2004). Mutation of GATA3 in human breast tumors. *Oncogene* **23**: 7669–7678.
van de Vijver MJ, He YD, van't Veer LJ, Dai H, Hart AA, Voskuil DW *et al.* (2002). A gene-expression signature as a predictor of survival in breast cancer. *N Engl J Med* **347**: 1999–2009.
van't Veer LJ, Dai H, van d V, He YD, Hart AA, Mao M *et al.* (2002). Gene expression profiling predicts clinical outcome of breast cancer. *Nature* **415**: 530–536.
Wang Y, Klijn JG, Zhang Y, Sieuwerts AM, Look MP, Yang F *et al.* (2005). Gene-expression profiles to predict distant metastasis of lymph-node-negative primary breast cancer. *Lancet* **365**: 671–679.
Yan W, Cao QJ, Arenas RB, Bentley B, Shao R. (2010). GATA3 inhibits breast cancer metastasis through the reversal of epithelial–mesenchymal transition. *J Biol Chem* **285**: 14042–14051.
Zhou M, Ouyang W. (2003). The function role of GATA-3 in Th1 and Th2 differentiation. *Immunol Res* **28**: 25–37.

Supplementary Information accompanies the paper on the Oncogene website (http://www.nature.com/onc)

8314–8328 *Nucleic Acids Research, 2011, Vol. 39, No. 19* *Published online 5 July 2011*
doi:10.1093/nar/gkr339

Mechanisms of translational regulation by a human eIF5-mimic protein

Chingakham Ranjit Singh[1], Ryosuke Watanabe[1], Donghui Zhou[2], Martin D. Jennings[3], Akira Fukao[4], Bumjun Lee[1], Yuka Ikeda[1], John A. Chiorini[5], Susan G. Campbell[3], Mark P. Ashe[3], Toshinobu Fujiwara[4], Ronald C. Wek[2], Graham D. Pavitt[3] and Katsura Asano[1,*]

[1]Molecular Cellular and Developmental Biology Program, Division of Biology, Kansas State University, Manhattan, KS 66506, [2]Department of Biochemistry and Molecular Biology, Indiana University School of Medicine, Indianapolis, IN 46202, USA, [3]Faculty of Life Sciences, The University of Manchester, Manchester, M13 9PT, UK, [4]Department of Chemical Science and Engineering, Graduate School of Engineering, Kobe University, Kobe 657-8501, Japan and [5]NIDCR, NIH, Bethesda, MD 20892, USA

Received March 2, 2011; Revised April 22, 2011; Accepted April 25, 2011

ABSTRACT

The translation factor eIF5 is an important partner of eIF2, directly modulating its function in several critical steps. First, eIF5 binds eIF2/GTP/Met-tRNA$_i^{Met}$ ternary complex (TC), promoting its recruitment to 40S ribosomal subunits. Secondly, its GTPase activating function promotes eIF2 dissociation for ribosomal subunit joining. Finally, eIF5 GDP dissociation inhibition (GDI) activity can antagonize eIF2 reactivation by competing with the eIF2 guanine exchange factor (GEF), eIF2B. The C-terminal domain (CTD) of eIF5, a W2-type HEAT domain, mediates its interaction with eIF2. Here, we characterize a related human protein containing MA3- and W2-type HEAT domains, previously termed BZW2 and renamed here as eIF5-mimic protein 1 (5MP1). Human 5MP1 interacts with eIF2 and eIF3 and inhibits general and gene-specific translation in mammalian systems. We further test whether 5MP1 is a mimic or competitor of the GEF catalytic subunit eIF2Bε or eIF5, using yeast as a model. Our results suggest that 5MP1 interacts with yeast eIF2 and promotes TC formation, but inhibits TC binding to the ribosome. Moreover, 5MP1 is not a GEF but a weak GDI for yeast eIF2. We propose that 5MP1 is a partial mimic and competitor of eIF5, interfering with the key steps by which eIF5 regulates eIF2 function.

INTRODUCTION

During translation initiation, eukaryotic initiation factors (eIFs) assemble initiator methionyl tRNA$_i^{Met}$ (Met-tRNA$_i^{Met}$) and m^{7}G-capped mRNA with the 40S ribosome subunit, precisely matching the tRNA$_i^{Met}$ anticodon to the mRNA start codon at the 40S ribosomal P-site (1,2). This translation process occurs in multiple steps. First, the heterotrimeric factor eIF2 (composed of α, β and γ subunits) binds Met-tRNA$_i^{Met}$, a process that is dependent on GTP being bound to the γ subunit of eIF2. The resulting eIF2/GTP/Met-tRNA$_i^{Met}$ ternary complex (TC) is incorporated into the 43S pre-initiation complex (PIC), which also contains eIF1A, eIF1, eIF3 and eIF5. The m^{7}G-capped mRNA is then activated and is recruited to the 43S PIC by eIF4F, composed of the cap binding protein eIF4E, adaptor eIF4G and mRNA helicase eIF4A, forming the 48S PIC that includes the 40S subunit located at the 5′-end of the mRNA. The PIC

*To whom correspondence should be addressed. Tel: +1 785 532 0116; Fax: +1 785 532 6653; Email: kasano@ksu.edu
Present addresses:
Susan G. Campbell, Biosciences Department, Faculty of Health and Wellbeing, Sheffield Hallam University, S1 1WB. UK.
Present addresses:
Toshinobu Fujiwara, Institute of Microbial Chemistry Laboratory of Disease Biology, 3-14-23, Kamiosaki, Shinagawa-ku Tokyo, 141-0021, Japan and Precursory Research for Embryonic Science and Technology, Japan Science and Technology Agency, 4-1-8 Honcho, Kawaguchi, Saitama 332-0012, Japan.
Present addresses:
Akira Fukao, Institute of Microbial Chemistry Laboratory of Disease Biology, 3-14-23, Kamiosaki, Shinagawa-ku Tokyo, 141-0021, Japan, and Research Fellow of the Japan Society for the Promotion of Science.

The authors wish it to be known that, in their opinion, the first two authors should be regarded as joint First Authors.

then scans along the 5′-leader of the transcript until the start codon of the mRNA base-pairs to the $tRNA_i^{Met}$ anticodon in the P-site of the ribosome. The concerted actions of the assembled eIFs coupled to the eIF2 GTPase activation (GAP) function catalyzed by the N-terminal domain (NTD) of eIF5 are thought to provoke conformational changes within the PIC, promoting the release of most eIFs, including eIF1, eIF2 and eIF5. The second GTP binding factor eIF5B then mediates the joining of the 60S subunit to form an 80S initiation complex, which is then ready to accept the second aminoacyl tRNA into the ribosomal A-site during the elongation phase of translation. eIF2 is released from the PIC as the GDP-bound form, which is reactivated to the GTP-form by eIF2B-catalyzed guanine nucleotide exchange, allowing for subsequent rounds of translation initiation. eIF5 appears to be ejected from the PIC in complex with eIF2-GDP, and antagonize eIF2B-catalyzed eIF2 reactivation (3) via its GDP dissociation inhibition (GDI) activity (4).

Many critical protein–protein interactions mediating the eukaryotic translation initiation process involve the HEAT domain, a globular domain comprising several repeats of conserved anti-parallel α-helical structures (5). For example, mammalian eIF4G molecules possess three distinct HEAT domains termed MIF4G, MA3 and W2 (Figure 1A). The MIF4G and MA3 domains of eIF4G together form a binding pocket for a single molecule of eIF4A, thereby regulating mRNA recruitment and scanning (6), whereas the last W2 domain is the binding site for Mnk eIF4E kinase (7) (Figure 1A). Mammalian eIF4G also possesses an unstructured N-terminal segment capable of binding poly(A) binding protein (PABP) and the m^7G-cap binding subunit, eIF4E. W2-type HEAT domains (W2-CTDs) are also found in the C-terminal segments of eIF5 and eIF2Bε but these are substrate binding sites for the lysine-rich N-terminal half of the eIF2β subunit (8,9). The role of W2-CTDs of eIF5 and eIF2Bε in the regulation of eIF2 activity has been well-established. The W2-CTD of eIF2Bε functions in guanine nucleotide exchange on eIF2 (10), whereas the W2 domain in eIF5 mediates the formation of a multifactor complex (MFC) with eIF1, eIF2-GTP, eIF3 and $Met\text{-}tRNA_i^{Met}$ (9,11). Finally the eIF5 W2-CTD together with the adjacent N-terminal linker region is responsible for the GDI activity against eIF2-GDP (3,4).

Two distinct copies of eIF4G are found in most eukaryotes examined so far. However, vertebrates encode a third eIF4G-like species termed p97/NAT1/DAP5 (Figure 1A). This protein lacks the N-terminal segment but contains the three HEAT domains analogous to mammalian eIF4G. Thus, p97/NAT1/DAP5 is a macromolecular

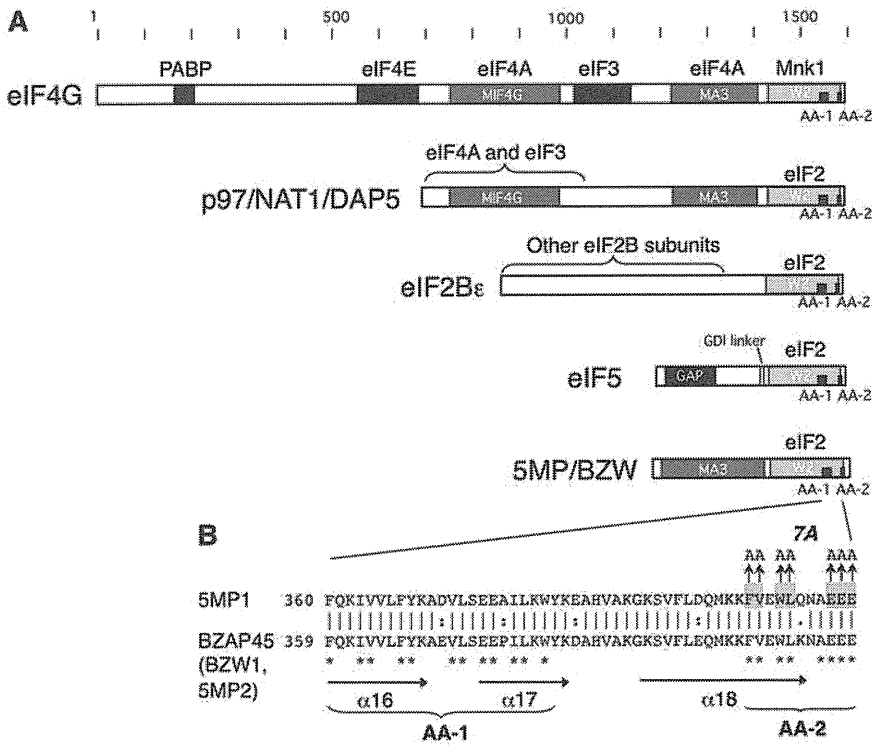

Figure 1. HEAT domain-containing translation initiation factors and regulators. (**A**) Primary structures of human eIF4G1, p97/NAT1/DAP5, 5MP1/BZW2 and yeast eIF2Bε and eIF5 are drawn to scale with filled boxes indicating segments known to interact with their partners listed across the top. Bracket indicates an approximate area of interaction with indicted partners. Light gray boxes indicate the W2 domains, with short thick lines representing the location of AA-boxes 1 and 2 (AA-1, AA-2, respectively). Gray boxes indicate other HEAT domains. (**B**) Alignment of C-terminal parts of amino acid sequences (starting with residue numbered to the left) from human 5MP1/BZW2 and 5MP2/BZW1/BZAP45. Asterisks indicate residues making up AA-boxes, while vertical arrows indicate mutations in *7A*. Horizontal arrows indicate the location of α-helices predicted from the homology with eIF4G.

mimic of the eIF4G C-terminal half (12,13), and it has been implicated in the modulation of translation for specific mRNAs (14). Interestingly the DAP5-CTD 3D structure is very similar to that of the W2-CTDs of eIF5 and eIF2Bε, and in common with these factors, but unlike eIF4G, DAP5 also binds to eIF2β (15).

In this study, we characterize another human HEAT domain-containing protein that is related to eIF5, known as BZW or MA3+W2 protein (Figure 1A) (16). Human BZW1 and BZW2 share 72% sequence identity and contain two HEAT domains, MA3 and W2 (hence the family name), comprising 10 and 8 α-helices that correspond to five and four HEAT repeats, respectively (http://famshelp.gsc.riken.jp/famsbase). While BZW1 was characterized as a transcription factor termed BZAP45 (17), its GFP-fusion form is localized in the cytoplasm (18). In addition, a single MA3+W2 protein is found in *Drosophila melanogaster* and is termed Krasavietz (Kra) (also known as eIF5C, Exba, or Ecp). Lee *et al.* (19) presented evidence that Kra co-migrates with 40S ribosomes and interacts with eIF2β more weakly than eIF5, and that Kra AA-box 1 and 2 mutations weaken this interaction with eIF2β. Furthermore, Kra reduces luciferase expression in rabbit reticulocyte lysate (RRL) (19). Interestingly, the *Drosophila Kra* mutants are defective in long-term memory (20) and consistent with this, Kra is implicated in neuronal development and interacts with Shot, the cytoskeletal element that links F-actin and microtubules required for axon formation (19).

The above-mentioned study of Kra protein suggests that all W2-containing proteins (eIF5, eIF2Bε, p97/NAT1/DAP5 and BZW/Kra), except eIF4G, bind eIF2. Because the eIF5-NTD that activates eIF2 GTPase in response to start codon selection is not present in the BZW proteins (Figure 1A), we hypothesized that BZW/Kra may serve as a mimic or competitor of eIF2Bε or an antagonist of eIF5 functions in translation. Here we tested these predictions and provide evidence from multiple systems (RRL, mammalian cells and yeast) that BZW2 does indeed antagonize eIF5 functions with eIF2 to modulate both general translation and the translation of specific genes at multiple steps. BZW stands for *b*asic leucine-*z*ipper with a *W*2 domain, although the conserved lysine/arginine and leucine residues that were characterized as basic leucine-zipper (17) are in fact a part of HEAT repeats that make up a MA3 domain (16). Based on this study emphasizing its role as a competitive inhibitor of eIF5 function by macro-molecular mimicry, we thus designate the BZW proteins as the eIF5-mimic proteins (5MPs), and rename human BZW2 and BZW1 as 5MP1 and 5MP2, respectively.

MATERIALS AND METHODS

Plasmids and yeast strains

Plasmids used in this study and oligodeoxyribonucleotides used for their constructions are listed in Supplementary Tables S1 and S2, respectively. Details of their construction and yeas strains used are described in Supplementary Data.

Yeast methods

We used the standard genetic/ molecular biology techniques and prepared yeast growth media. Immunoaffinity purification of FLAG-tagged protein complexes was performed as described (3,11,21).

In vitro protein–protein interaction assay

eIF3 and eIF2 were purified from HeLa cells (kindly provided by J. Hershey and M. Sokabe). FL-5MP1 and its mutants were purified from H2557 transformants carrying pEMBL-FL-5MP1 and its derivatives, that had been grown in synthetic complete galactose medium lacking uracil (SCGal-ura), as described (22). Recombinant eIF5 was purified by G50 column fractionation after thrombin treatment of GST-human eIF5 (23).

To perform GST pull-down assays, GST-fusion proteins were expressed in BL21(DE3) transformants carrying the relevant pGEX- series of plasmids (Table S1), purified in one-step with a glutathione resin and used immediately for the interaction with their purified partners, essentially as described (24). In each experiment and its repeats, we used a fixed amount of GST-fusion proteins (5 μg each of GST, GST-5MP1 and GST-5MP1-7A in Figure 2A and D; 5 μg GST, 3 μg each of GST-eIF2α and -eIF2β in Figure 2B) and 10 times less (in molarity) purified partners. For the latter, we used 1 μg human eIF2 (Figure 2A) or 8 μg human eIF3 (Figure 2D), or 300 ng of FL-5MP1 or FL-5MP1-7A (Figure 1E). After incubation, protein complexes adsorbed to the resin were washed, dissolved into a SDS–PAGE buffer and analyzed by immunoblotting.

Analysis of 43S/48S PIC in RRL

m^7G-capped luciferase mRNA was synthesized and purified using the mMegascript mMessage kit (Ambion) and SmaI-linearized plasmid pRG166 as template (25). Translation reaction (20 μl) was performed with RRL in the presence of cold amino acids using 2.5 ng cap-LUC mRNA, as recommended by the manufacturer (Promega). After incubation at 30°C for 20 min, the sample was supplemented with 160 ng BSA or FL-5MP1 and incubated for an additional hour. The samples were fixed with 1% HCHO on ice for 30 min, quenched with 0.1 M glycine and layered on 5–40% sucrose gradient containing 20 mM Tris–HCl (pH 7.5), 100 mM NaCl and 1 mM $MgCl_2$. After ultracentrifugation at 39 000 rpm for 4.5 h, the gradient sample was fractionated by ISCO gradient fractionator. The top nine fractions were precipitated and analyzed by immunoblotting, together with an in-put control and purified recombinant eIF5 as references.

Polysome profiling of the HeLa cells

HeLa cells grown in 6-cm petri dish containing 2 ml complete Dulbecco's modified Eagle's medium (D-MEM, GIBCO) supplemented with 10% fetal bovine serum (GIBCO) were transfected with indicated plasmids using PolyFect Transfection Reagent (QIAGEN), and

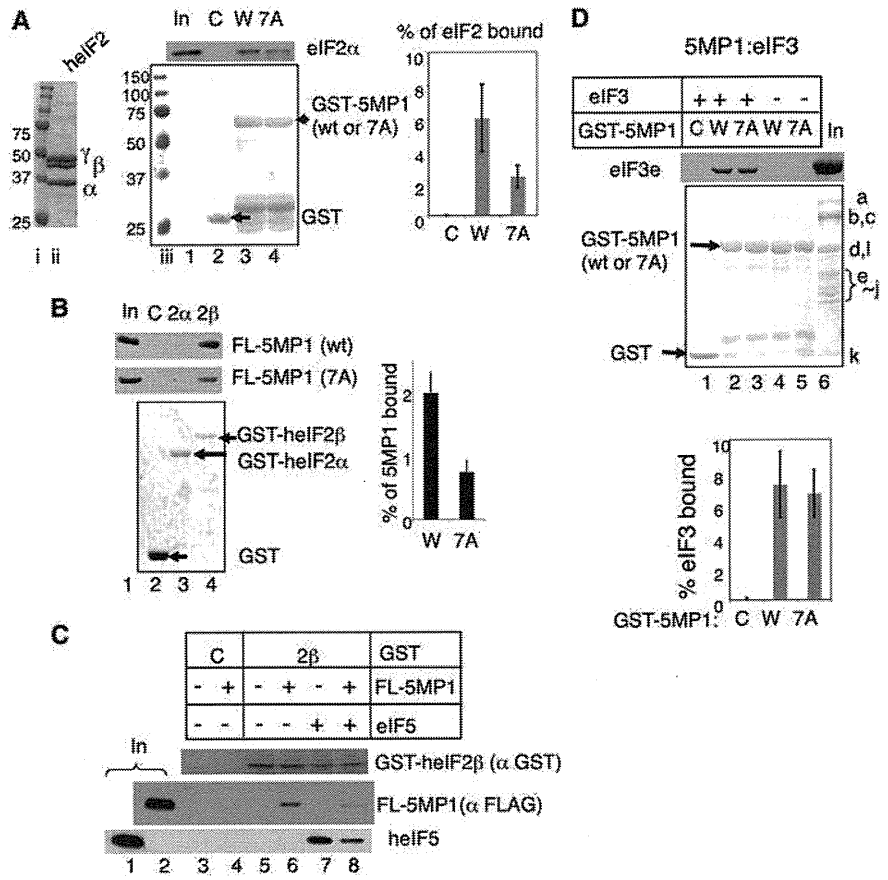

Figure 2. Human 5MP1/BZW2 interacts with eIF2 and eIF3. (**A**) Pulldown assays with GST-5MP1 (W, wild-type), its *7A* derivative (7A) or GST alone (C). The complexes with human eIF2 were analyzed with 10% in-put (In) control by immunoblotting using anti-eIF2α (Santa Cruz Biotech.) (top gel) followed by Ponceau S staining (bottom gel). Arrows in the bottom gel indicate the location of GST-fusions used. Lanes i and iii, size standards. Lane ii, human eIF2 used visualized by Coomassie staining. Graph summarizes percentage of eIF bound to GST-fusions used, with bars indicating SD. (**B**) Interactions of 5MP1 with individual eIF2 subunits fused to GST. GST-eIF2α (2α), and -eIF2β (2β) bound to FL-5MP1 (wt) or its *7A* version (7A) were analyzed with 2.5% in-put (lanes 1) by immunoblotting (top gels) with anti-FLAG M2 antibodies (Sigma), followed by Ponceau S staining shown on bottom and presented as in (A). C, control with GST alone. Graph indicates the percentage of FL-5MP1 or FL-5MP1-7A bound to GST-eIF2β, with bars denoting SD. (**C**) Competition assay. FL-5MP1 (200 ng) and/or human eIF5 (1.6 μg) were incubated with GST-heIF2β (2β) or GST alone (C) (1 μg) pre-adsorbed to glutathione resin, and the complex was precipitated and analyzed by immunoblotting with anti-GST (top), anti-FLAG (middle) and anti-heIF5 (bottom) antibodies, as in (A). Lane 1, 5% in-put of heIF5. Lane 2, 25% in-put of FL-5MP1. (**D**) Pulldown assays with GST-5MP1 and its *7A* derivative (7A) were performed with human eIF3, similar to (A), and analyzed with 50% in-put (In) control by immunoblotting using anti-eIF3e (41) antibodies (top gel), followed by Ponceau S staining (bottom gel). The results were presented as in (A). In the 'in-put' lane, eIF3 subunit names are identified to the right. Graphs summarize the percentage of eIF3 bound to GST-fusions used, with bars indicating SD.

after 24 h, the medium was replaced with 2 ml D-MEM (no serum) and the cells were incubated for additional 24 h. Then FBS (GIBCO) was added to 10% and the cells were collected for polysome profiling after 20 min. The collected cells (4×10^6 cells) were lysed in 500 μl lyse buffer (20 mM HEPES, pH 7.5, 100 mM KCl, 10 mM $MgCl_2$, 0.25% NP-40, 100 μg/ml cycloheximide, 100 U/ml RNase inhibitor, protease inhibitor cocktail) by passing through a sterile syringe with a 26 or 27 gauge needle several times. Then the lysate was cleared by a brief centrifugation (10 000*g*, 5 min) to remove non-ribosomal nuclear components, which otherwise increase the base-line of the profile towards the bottom of the gradient. Subsequently, 400 μl of the cleared lysate was layered on 5 ml 10–45% sucrose gradient (20 mM HEPES, 100 mM KCl, 10 mM $MgCl_2$) in 151–513 tubes and fractionated by centrifugation at 40 000 rpm for 1 h at 4°C in a Beckman MLS-50 rotor. The gradient was analyzed by the Biocomp Piston Gradient Fractionator™. The reminder of the lysate was used for checking the total protein yield by the Lowry method and immunoblotting with anti-RPL7 antibodies. As shown by anti-RPL7 immunoblot in Figure 4B, the total ribosome content of the lysate was not altered significantly by expression of 5MP1 under the conditions examined. We also confirmed by immunoblotting with these antibodies that the above-mentioned treatment of clearing the lysate does not affect the amount of ribosomes in the lysate and that the area shown by bracket in Figure 4C covers the entire polysome. Thus, the lysate clearing is essential in evaluating polysome abundance in mammalian cultured cells by densitometry under our experimental conditions.

ATF4 expression assay in MEF cell lines

Details of *ATF4* expression assay were reported previously (26). Briefly, MEF cells homozygous for *eIF2α-S51A* mutation obtained from Randall Kaufman (University of Michigan, Ann Arbor) were immortalized by infection of a recombinant retrovirus expressing simian virus 40 large T antigen. MEF cells were grown in 24-well plates in D-MEM (BioWhittaker) supplemented with 10% FBS, 2 mM glutamine, 1 mM nonessential amino acids, 100 units of penicillin per ml and 100 μg of streptomycin per milliliter. Plasmid transfections were performed by using the MEF cells at 40% confluency and the FuGENE tranfection reagent (Roche Applied Science). Cotransfections were carried out in triplicate by using the pCDNA plasmids, the *TK-ATF4-Luc* fusion plasmid (p759) and a *Renilla* luciferase plasmid (p851) serving as an internal control (Promega). After transfection (40 h), MEF cells were treated with thapisgargin (Tg) at 0.1 μM, for 6 h or with no ER stress. Dual luciferase assays were carried out as described by the Promega instruction manual (cat #E1960). Values shown in Figure 4D are a measure of a ratio of firefly versus *Renilla* luciferase units (relative light units, RLU), and represent the mean values of three independent transfections. We reproducibly obtained similar levels of *Renilla* LUC activity in wild-type and eIF2α-*S51A* MEFs, unless translation is strongly perturbed e.g. by high dose of Tg. Thus, the transfection efficiency is stable under our experimental conditions. At least two sets of independent experiments were performed to confirm reproducibility.

Fluorescent microscopy

Live yeast cells were mounted onto 0.5% poly-L-lysine–coated slides and visualized on a Leica SP5 confocal microscope with a 63 × 0.6–1.40 NA Plan Apochromat oil objective (Leica). Images were acquired using Application suite 1.6.3 (Leica). For densitometric analysis, a merged ~80 Z-series projection image was taken and analyzed using NIH ImageJ software. For data analysis, we took Z-projection images of cells from at least three independent mid-log cultures that had been grown in SCGal-ura.

RESULTS

5MP1 interacts with human eIF2 and eIF3 *in vitro*

We first wished to test if the human 5MP1 protein binds to eIF2. For this purpose, we incubated eIF2 purified from HeLa cells (Figure 2A, lane ii) with glutathione resin pre-adsorbed with GST-5MP1 fusion protein, or with GST alone. Associated proteins were then analyzed by immunoblotting with anti-eIF2α antibodies. eIF2α was detected in the complex with GST-5MP1 (Figure 2A, lane 3, top gel); thus, GST-5MP1 interacts with human eIF2. To test if the 5MP1 interaction with eIF2 depends on AA-boxes that characterize the W2 domain (Figure 1B), we introduced 7 alanine-substitutions to the AA-box 2 of GST-5MP1. This mutation, here called 5MP1-*7A*, reduced the interaction between GST-5MP1 and eIF2 by >2-fold ($P = 0.027$, $n = 4$) (Figure 2A, lane 4; quantified in the graph on top). This shows that AA-box 2 of 5MP1 contributes to the eIF2 binding site similar to the AA-box motifs in eIF5, eIF2Bε and Kra.

Because eIF5, eIF2Bε and Kra interact with eIF2 via the eIF2β subunit (8,19,27), we also examined if 5MP1 binds directly to eIF2β. As shown in Figure 2B (top gel) purified FLAG-tagged 5MP1 (FL-5MP1) bound specifically to GST-fused human eIF2β (GST-eIF2β), but not to GST-fused human eIF2α (lanes 2–4). Again, the *7A* mutation in 5MP1 reduced its interaction with GST-eIF2β by 2-fold ($P = 0.002$, $n = 6$) (Figure 2B, lower gel and graph). Thus, 5MP1 interacts with eIF2β at least partially via its AA-box 2 motif, suggesting eIF2β represents a major site of interaction between 5MP1 and eIF2.

Since the observed interaction between 5MP1 and eIF2β proceeds via the same AA-box 2 motif as eIF5 uses to bind eIF2β, we hypothesize that 5MP1 and eIF5 may compete with each other for binding to eIF2β. To test this idea directly *in vitro*, we incubated GST-eIF2β with 5MP1 and eIF5, alone or in combination. As shown in Figure 2C (middle gel), human eIF5 outcompeted the binding of FL-5MP1 to GST-eIF2β (compare lanes 6 and 8). Interestingly, the amount of human eIF5 bound to GST-eIF2β was also reduced by the presence of FL-5MP1 (Figure 2C, bottom gel, lane 8), even though eight times more eIF5 than FL-5MP1 was present. This suggests that interactions of eIF2β with eIF5 and 5MP1 are mutually exclusive, and 5MP1 may act as a competitive inhibitor of eIF5.

The eIF5 W2 domain also interacts with eIF3. Therefore, we next examined whether 5MP1 could also bind to purified eIF3. The eIF3 preparation used here contains all 13 subunits including eIF3e subunit, which was used for immunodetection of eIF3 in this study. As shown by immunoblotting with anti-eIF3e, eIF3 specifically co-precipitated with GST-5MP1 but not with GST alone (Figure 2D, lanes 1 and 2). The absence of anti-eIF3e signals with GST-5MP1 or -5MP1-7A alone confirms the authenticity of the eIF3 subunit detected here (lanes 4 and 5). Importantly, this interaction was not compromised by the AA-box 2 mutation in the 5MP1-*7A* protein (lanes 2 and 3, see graph to the right for quantification), indicating that this mutation specifically affects the interaction with eIF2. These results together indicate that 5MP1 can interact with both eIF2 and eIF3, similar to the eIF5 W2 domain.

5MP1 inhibits translation in RRL

Next, we examined the effect of 5MP1 on protein synthesis using a cell-free RRL translation assay. As shown in Figure 3A (inset), purified FL-5MP1 repressed ^{35}S-luciferase synthesis in RRL programmed with capped luciferase (*LUC*) mRNA (lane 2), while the addition of equivalent amount of BSA did not (lane 1). The titration experiments in Figure 3A indicated that ~40 ng or 0.8 pmol of FL-5MP1 is required for nearly full inhibition: Because the RRL used here contains 7

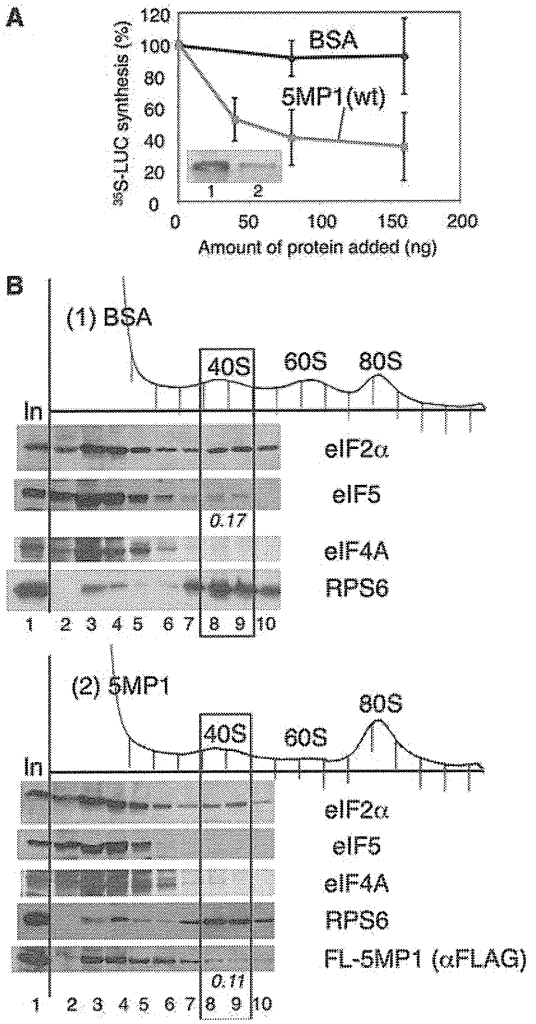

Figure 3. 5MP1/BZW2 inhibits cell-free translation in RRL. (**A**) Cell-free translation of ^{35}S-luciferase (LUC) was performed in the presence of different amounts of indicated proteins in 10 µl RRL programmed with 1.25 ng capped LUC mRNA. The reaction was run at 30°C for 1 h in the presence of [^{35}S]-methionine. Inset shows autoradiography indicating the amount of LUC production. Graph shows the plot of relative ^{35}S-LUC synthesis against the amount of proteins added from at least three independent experiments, with bars indicating SD. (**B**) RRL programmed with cap-LUC mRNA was supplemented with 160 ng BSA (panel 1) or FL-5MP1 (panel 2) and incubated for 1 h. The samples were fixed with HCHO and resolved by sucrose gradient-velocity sedimentation. Fractions were analyzed by immunoblotting with antibodies indicated to the right. In, 10% in-put RRL used. The amounts of eIF5 or FL-5MP1 (in picomoles) associated with the 40 S subunit are listed to the bottom of the gel.

and 3 pmol of eIF2 and eIF5, respectively (data not shown), translational inhibition by 5MP1 is quite efficient.

To address the mechanisms by which 5MP1 can inhibit translation in RRL, we fractionated RRL programmed for luciferase mRNA translation with or without FL-5MP1 by sucrose gradient–velocity sedimentation. As shown in Figure 3B, anti-eIF2α immunoblot of gradient fractions of control RRL revealed that eIF2 was across the gradient; however, there was a specific peak indicating eIF2 comigration with the 40S subunit (panel 1). The amount of eIF2 comigrating with the 40S was not significantly affected by 5MP1 addition to RRL (Figure 3B, panels 1 and 2), a trend that was confirmed among many repeated experiments. Importantly, the addition of FL-5MP1 reduced eIF5 binding to the ribosome to levels that were not detectable (Figure 3B, panels 1 and 2). The eIF5 comigration with the 40S subunit in the control RRL appears to reflect specific interaction, as the 40S fractions do not contain mRNA helicase eIF4A, which does not bind stably to the 40S subunit (Figure 3B, panels 1 and 2). Instead, we found that FL-5MP1 appeared to comigrate with the 40S subunit (Figure 3B, panel 2, bottom panel) at a level equivalent to that of eIF5 in the control RRL (panel 1). These results, combined with the competition experiments shown in Figure 2D, suggest that 5MP1 may competitively inhibit eIF5 recruitment to the 40S subunit.

Human 5MP1 is capable of repressing translation and modulating *ATF4* expression in mammalian cells

To express 5MP1 in mammalian cells, we cloned 5MP1 and its GFP-fusion and *7A* mutant derivatives under a CMV promoter (pCDNA-5MP1 and derivatives in Supplementary Table S1). Transfection of 5MP1-GFP led to cytoplasmic GFP localization as judged by fluorescent microscopy (Figure 4A), in agreement with the cytoplasmic location of 5MP2/BZW1 reported previously (18). pCDNA-5MP1 and its derivatives express a similar level of 5MP1 in transfected HeLa cells (Figure 4B), and immunoblotting indicated that the expressed 5MP1 proteins were found specifically in the cytoplasmic, but not in the nuclear fractions of HeLa cell extracts (data not shown). The transfection of pCDNA-5MP1 expressing 5MP1 alone led to a small reduction in the polysome content of the cells, especially the highly sedimenting polysomes (Figure 4C, compare panels 1 and 2). Given that 5MP1 is cytoplasmic and its expression impacts upon polysome profiles, the data are consistent with the idea that 5MP1 modulates translation in mammalian cells.

The relatively weak effect of enhanced 5MP1 expression upon general protein synthesis (Figure 4C) led us to address whether elevated 5MP1 changes the translation of specific mRNAs. *ATF4* mRNA is translationally enhanced by phosphorylation of eIF2 in response endoplasmic reticulum (ER) stress, a process that can be triggered by addition of the well-characterized ER stress agent thapsigargin (Tg) (28). The regulation of *ATF4* translation depends on its upstream open reading frames (uORFs). In short, *ATF4* translation requires prior translation of uORF1, resumed 40S scanning, bypassing of uORF2 and re-initiation at *ATF4* AUG, whereas re-initiation at uORF2 prevents subsequent translation of *ATF4* (28). This choice is modulated by eIF2 phosphorylation, which transforms eIF2 into a competitive inhibitor of eIF2B, thereby reducing the cellular eIF2-GTP/Met-tRNA$_i^{Met}$ (TC) level and delaying TC binding to the re-initiating 40S subunit. This allows uORF2 to be bypassed during times of stress and instead, promotes re-initiation at *ATF4* located downstream. Thus, if

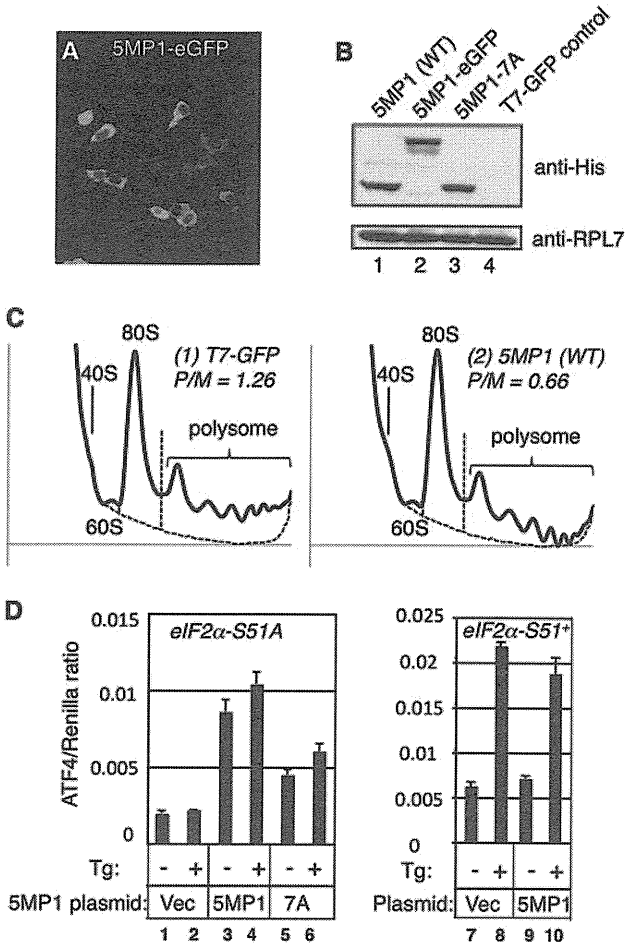

Figure 4. 5MP1/BZW2 controls general and *ATF4*-specific translation in mammalian cells (**A**) Fluorescence emitted from 293 T cells transfected with pCDNA-5MP1-GFP. (**B**) HeLa cells were transfected with plasmids indicated across the top and subjected for immunoblotting with antibodies indicated to the right. Anti-RPL7 was used as loading control. (**C**) Polysome profiles of serum-activated HeLa cells transfected with pCDNA-5MP1 (panel 2) or pT7-GFP control (panel 1) were monitored as described (29) with the P/M ratio presented on top right. Dotted line indicates an arbitrary base-line used to calculate P/M ratio. Identical base-line and scale in y axis were set for each set of experiments for accurate comparison. (**D**) Effect of 5MP1/BZW2 on *ATF4* expression. Wild-type (*eIF2α-S51*$^+$) MEF (Columns 7–10) or MEF homozygous for *eIF2α-S51*A (Columns 1–6) were triple-transfected with *ATF4-luc, Renilla* luciferase plasmind, and an empty vector (Vec), pCDNA-5MP1 (WT) or −7A (7A), treated with (+) or without (−) 0.1 μM Tg, and assayed for luciferase expression. Graphs in (D) show the ratio of expression from *ATF4-luc* to that from the Renilla *luc* with bars indicating SD (n = 3). These are a typical result of reproduced experiments.

5MP1 modulates TC recruitment or abundance, this may alter re-initiation and affect *ATF4* expression in the absence of eIF2 phosphorylation.

ATF4 expression was measured by firefly luciferase activity from a transiently transfected *ATF-LUC* plasmid and was normalized by *Renilla* luciferase activity expressed from a second co-transfected plasmid. In mouse embryonic fibroblasts (MEF) containing an alanine mutation in the serine-51 phosphorylation site of eIF2α (eIF2α-*S51A*) there is no induction of *ATF4*-regulated luciferase activity in response to ER stress, emphasizing the specificity of this translational control (Figure 4D, Columns 1 and 2). As a control, the same Tg treatment induced *ATF4* expression >3-fold in MEF with wild-type eIF2α (*eIF2α-S51*$^+$) (Figure 4D, Columns 7 and 8). Expression of 5MP1 significantly increased the level of *ATF4* translation in the eIF2α-*S51A* cells independent of stress treatment (Figure 4D, Columns 3 and 4). However, 5MP1 expression did not increase *ATF4* expression in the *eIF2α-S51*$^+$ cells (Figure 4D, Columns 9 and 10). Interestingly, the increase in *ATF4* expression observed here with enhanced 5MP1 expression was alleviated partially by the *7A* mutation, and was observed to be independent of Tg treatment (Figure 4D, lanes 5 and 6). These results suggest that the alteration in 5MP1 interaction via the AA-box 2, perhaps with eIF2, can modulate *ATF4* translation by affecting TC activity or recruitment in mammalian cells.

Human 5MP1 can inhibit GDP dissociation from yeast eIF2

The data described thus far are consistent with the idea that 5MP1 can modulate translation initiation by binding to eIF2 and competitively excluding eIF5 through its W2 HEAT domain. This is consistent with a major function of the W2-CTD, which is to bridge the interaction between eIF2 and eIF3, hence mediating the formation of the MFC also containing eIF1 (11). Because the eIF5 GAP function requires the NTD that is not conserved in 5MP/BZW (30) it appeared highly unlikely that 5MP1 was a functional GAP, so this activity was not assessed. However, the W2-CTD of yeast eIF5, together with its juxtaposed linker region (LR), has also been described to inhibit GDP dissociation from eIF2: GDI activity (4). This activity opposes the guanine nucleotide exchange activity of eIF2B by stabilizing GDP binding. While our data so far suggest that 5MP is a competitive inhibitor of eIF5 function in promoting translation, because theW2-type HEAT domains (W2-CTD) of eIF2Bε, p97/NAT1/DAP5 and eIF5 are structurally similar to that of 5MP (Figure 1) and all interact with eIF2, it was also possible that 5MP1 is a mimic of eIF2Bε or acts to functionally replace this factor. Indeed, the W2-CTD of eIF2Bε is the catalytic domain that can function alone in a direct GEF assay (10). Therefore by assessing whether 5MP1 affects GDP dissociation, we were able to directly assess if it mimics either GEF (accelerates GDP release) or GDI (retards GDP release) functions of eIF2Bε and eIF5, respectively. For this purpose, we purified GST-5MP1 and its *7A* mutant derivative and examined their effect on GDP retention by yeast eIF2 in a standard assay examining the dissociation of [^{3}H]GDP from purified eIF2. As shown in Figure 5A, GDP dissociation was modestly, but significantly, reduced by wild-type 5MP1, but not by 5MP1-*7A*. Since GDP dissociation was not increased, as has been observed by adding eIF2Bε (10), this result indicates that 5MP1 is not a functional mimic of eIF2Bε. The retardation of GDP

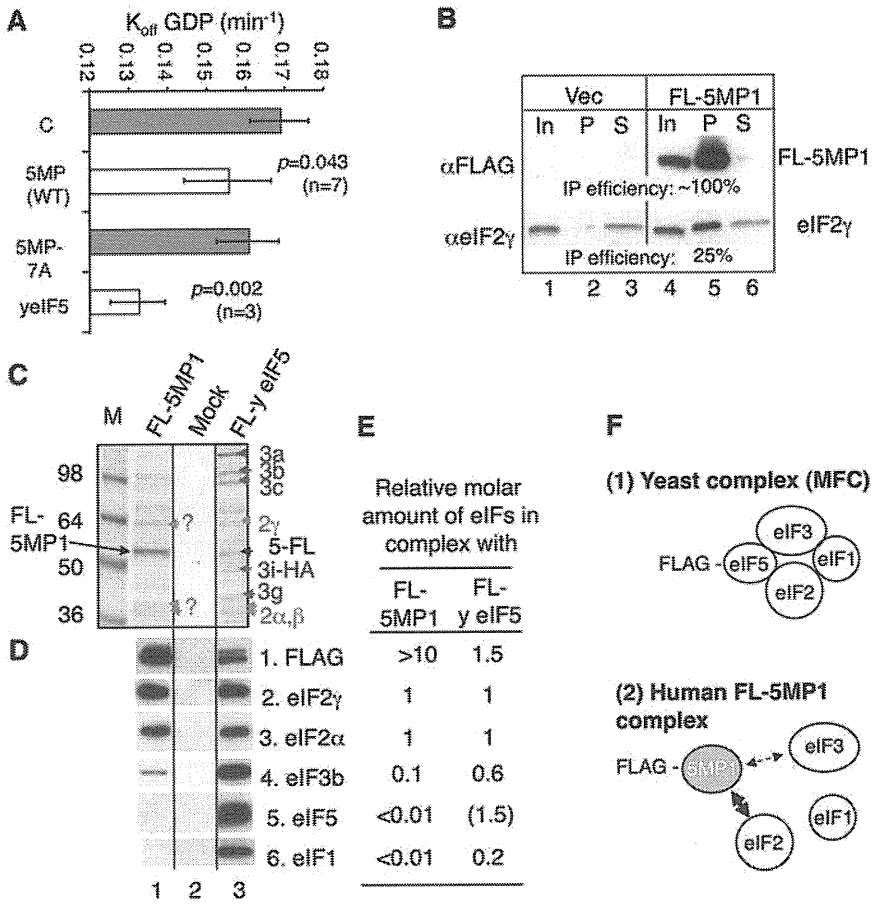

Figure 5. The GDI activity test of 5MP1/BZW2 and its interaction with eIFs in yeast *S. cerevisiae*. (**A**) GDI assay. Off-rates for eIF2-GDP was measured in the presence of indicated proteins fused to GST (4). C, Buffer control. Bars and line indicate mean and SD, respectively. Gray filled bars, not significantly different from buffer alone; unfilled bars are significant with *P*-value and the number of experiments (n) shown. (**B**) Immunoprecipitation. An amount of 200 μg of WCE prepared from H2557 transformants carrying an empty vector (Vec) or pEMBL-FL-5MP1 (FL-5MP1) which had been grown in SCGal-ura was used for anti-FLAG IP, and entire IP fractions (P), 20% in-put (In) and 10% supernatant (S) fractions were analyzed by immunoblotting with anti-FLAG (top) and anti-yeIF2α (SUI2) (bottom) antibodies. (**C** and **D**) Affinity-purification of FL-5MP1 complexes in yeast. Complexes containing the FLAG-tagged proteins listed across the top were purified from H2557 transformants carrying pEMBL-FL-5MP1 (lane 1) or a vector control (lane 2) and KAY50 (*TIF5-FL*) (lane 3), as described (11). The former two strains were grown in SCGal-ura medium and the latter was grown in YPD. Portions of the eluates were analyzed by Coomassie Blue staining (C) and immunoblotting with antibodies raised against yeast eIFs listed to the right (D). In (C), arrowheads indicate the positions of eIF subunit identified. Gray labels, eIF2 subunits; Iron labels, eIF3 subunits; Black labels, yeIF5-FL (5-FL) or FL-5MP1. (**E**) Table summarizes the relative molar ratio of co-purifying factors, compared to the molarity of eIF2 (Rows 2 and 3) as defined as 1. These ratios were determined in reference to purified external standards as described previously (3,21). (**F**) Models depicting the interaction of FLAG-yeIF5 (panel 1, oval labeled eIF5) and FLAG-human 5MP1 (panel 2, gray oval) with yeast factors (open ovals). Direct contact, strong interaction; arrow, intermediate interaction; dotted arrow, weak interaction.

dissociation by 5MP1 was weaker than by GST-yeast eIF5 (yeIF5) (Figure 5A). Thus, 5MP1 appears to act as a mimic/competitor of the GDI activity, in addition to its macromolecular mimicry and competitive binding to eIF2 and antagonizing pre-initiation factor complex formation. These activities are potentially opposed to each other, as weak GDI function with eIF2-GDP could promote nucleotide exchange and enhance eIF2 recycling. However binding to eIF2 TC may prevent its productive recruitment to 40S ribosomes and reduce translation initiation. We therefore decided to examine effects of 5MP1 expression in yeast, as this has been a sensitive *in vivo* system for examining translation and its control.

5MP1 interacts with eIF2 and weakly with eIF3 in *Saccharomyces cerevisiae*

We expressed 5MP1 in yeast to take advantage of various assays established for analyzing eIF2 regulation in translational control. We first examined its interaction with the yeast translation initiation factor (yeIF) components *in vivo*. When overexpressed from the *GAL* promoter, FLAG-tagged 5MP1 (FL-5MP1) expressed ~25 times more abundantly than endogenous eIF5 or eIF2 in galactose medium. Anti-FLAG immunoprecipitation (IP) indicated that ~25% of total eIF2 is specifically associated with the galactose-induced FL-5MP1 (Figure 5B). We previously reported that ~60% of yeIF5, expressed

in single-copy, is associated with total eIF2 (21). Because the level of 5MP1/yeIF2 complex was lower than that of yeIF5/yeIF2 complex even when 5MP1 was overexpressed, the interaction of 5MP1 with yeast eIF2 is likely to be weaker than that between yeast eIF5 and eIF2 *in vivo*.

To investigate the interaction of other MFC components with FL-5MP1, we analyzed the eIF constituents of FL-5MP1 complexes that were purified by anti-FLAG affinity chromatography (Figure 5C, lane 1). As shown in Figure 5C, Coomassie blue staining of the gel indicated that the FL-yeIF5 immunopurified sample contains yeast eIF3, eIF5 and eIF2 (lane 3), representing part of the MFC, as reported previously (3,11,21). The FL-5MP1 immunopurified sample contained three proteins, which appeared to comigrate with the three eIF2 subunits (? in lane 1) in quantities roughly equivalent to those found in the FL-yeIF5 sample (gray arrowheads in lane 3). The identity of six of the MFC polypeptides was confirmed by immunoblotting (Figure 5D), and the relative molar abundances of eIF1, eIF2, eIF3 and eIF5 (compared to eIF2 subunits) were determined using purified recombinant proteins as external standards and presented in Figure 5E. These data showed that the FL-5MP1 (lane 1) and FL-yeIF5 (lane 3) immunopurified fractions contained similar amounts of co-purifying yeIF2 (Rows 2 and 3). Because much more FL-5MP1 was present in lane 1 than FL-yeIF5 found in lane 3 (Figure 5D and E, Row 1), this also highlighted that the FL-5MP1 interaction with yeIF2 is likely to be weaker than yeIF5/yeIF2 interaction. Importantly, yeIF5 was not detected at all in the FL-5MP1 complex (Figure 5E, Row 5) providing *in vivo* evidence that 5MP1 and eIF5 form mutually exclusive complexes with eIF2 (Figure 5F). This is consistent with each factor competing for the same interaction site on eIF2. In addition, a small but significant amount of yeIF3 was found associated with immunopurified FL-5MP1 (Figure 5D and E, Row 4), consistent with the observed 5MP1 interaction with human eIF3 (Figure 2D). However, no yeIF1 was associated with FL-5MP1, indicating that the 5MP1 cannot mimic the role of eIF5 in MFC formation (Figure 5D and E, Row 6).

5MP1 decreases eIF2 localization to eIF2B-associated bodies in yeast

Despite the substantial interaction observed between 5MP1 and yeIF2, the 5MP1 overexpression did not retard the yeast growth rate. To detect any perturbation in translation initiation *in vivo*, especially one related to eIF2 activity, we took an independent cell biology approach. A significant fraction of yeast mother cells usually harbor a single cytoplasmic body containing eIF2B (termed the eIF2B body) (34). These are distinct from other cytoplasmic foci, e.g. the processing bodies, EGP bodies or stress granules (31–33). Photobleaching experiments have shown that eIF2B is a fixed component of this body, while eIF2 is more dynamic, shuttling through the body. Under conditions that reduce GEF activity (stress or eIF2B mutations); the rate of eIF2 cycling through the body was significantly reduced, suggesting that the eIF2B bodies represent a concentrated site of nucleotide exchange (34). We predicted that if 5MP1 interacts with yeIF2 and inhibits translation, this would decrease the shuttling of yeIF2 through the eIF2B bodies. To test this idea, we introduced the *GAL*-5MP1 plasmid, or hc yeIF5 plasmid as a control, to strains bearing GFP-tagged yeIF2Bγ or GFP-tagged yeIF2α. The introduction of neither plasmid affected the frequency or size of the eIF2B body in the eIF2B-GFP strain (data not shown). In contrast, when introduced to YMK883 expressing GFP-eIF2α (Figure 6A inset), we observed that both the *GAL*-5MP1 and hc yeIF5 plasmids reduced the proportion of cells eliciting medium to strong GFP-yeIF2 signals present in the bodies (Figure 6A, graph, Rows 3 and 4; Figure 6B, Row 3), suggesting that eIF2 activity is reduced by the overexpression of 5MP1 or yeIF5. This thesis is supported by additional statistical analyses of the microscopic data; we measured the proportion of the GFP-yeIF2 signal intensity localized in the eIF2B body, compared to total GFP-yeIF2 signal intensity in each cell across an entire population of cells. This value decreased from 9.2% (vector control) to 2.7 and 4.0% by overexpression of yeIF5 and 5MP1, respectively (Figure 6B, Row 4). Importantly, the reduced localization was restored to normal by introduction of the AA-box 2 mutation to the *GAL*-5MP1 construct (Figure 6A, column d; Figure 6B, Rows 3 and 4). This result is the opposite of the impact of conditions that lead to induced or constitutive eIF2α phosphorylation, under which increased association of GFP-yeIF2 with eIF2B bodies was observed (34). Thus, the result shown in Figure 6B suggests that overproduced 5MP1 reduces the rate of shuttling of yeIF2 through the eIF2B body, by inhibiting yeIF2 recruitment to eIF2B bodies, directly or indirectly, in a manner that is dependent upon the 5MP1 AA-box 2. This observation is consistent with excess yeIF5 or 5MP1 exerting an overall negative effect on translation initiation rates in cells. We explored this idea next using a genetic strategy.

5MP1 increases the yeast general control response independently of Gcn2p activation

We reasoned that if 5MP1 directly binds yeIF2, then it might influence *GCN4* translation, which is activated by alterations in TC levels and recruitment in a mechanism similar to that described for *ATF4* above. For example, 5MP1 might trigger preferential translation of *GCN4*, due to the depletion of eIF2 from the TC (35). This would be entirely consistent with the effect of 5MP1 on *ATF4* translation in the absence of eIF2 phosphorylation (Figure 4D). Phosphorylation of eIF2 in response to amino acid starvation in yeast, via the Gcn2p eIF2α kinase, typically lowers TC abundance and delays the re-initiation process that otherwise occurs on an uORF in the *GCN4* leader, and instead increases re-initiation at the *GCN4* ORF. We overexpressed 5MP1 to investigate whether the increased eIF2 binding could deplete the TC leading to enhance *GCN4* translation in a Gcn2p-independent manner. In practice, this entailed the